

THE 11TH GEORGE BROWN LECTURE

# Clay minerals for nanocomposites and biotechnology: surface modification, dynamics and responses to stimuli<sup>†</sup>

H. HEINZ\*

*Department of Polymer Engineering, University of Akron, Akron, OH 44325, USA*

*(Received 17 January 2012; revised 3 April 2012; Editor: John Adams)*

**ABSTRACT:** Clay minerals find a wide range of application in composites, paints, drilling liquids, cosmetics, and medicine. This article reviews chemical and physical properties of natural and organically modified clay minerals to understand the nanometre-scale structure, surface characteristics, and application in functional materials. The relation between fundamental properties and materials design is emphasized and illustrated by examples. The discussion comprises the following: an overview; surface structure and cation density; solubility and solubility reversal by surface modification; the degree of covalent and ionic bonding represented by atomic charges; the distribution of metal substitution sites; measurements and simulations of interfacial properties at the nanometre scale; self-assembly, packing density, and orientation of alkylammonium surfactants on the clay mineral surface; the density and chain conformation of surfactants in organic interlayer spaces; the free energy of exfoliation in polymer matrices and modifications by tuning the cleavage energy; thermal transitions, diffusion, and optical responses of surfactants on the mineral surface; elastic moduli and bending stability of clay layers; and the adsorption mechanism of peptides onto clay mineral surfaces in aqueous solution. Potential applications in biotechnology and other future uses are described.

**KEYWORDS:** clay minerals, surfactants, dispersion, simulation, nanomechanics, nanocomposites, biotechnology.

Clay minerals are widely used in drilling liquids, cosmetics, detergents and, more recently, in nanotechnology and biotechnology (Van Olphen, 1977; Ray & Bousmina, 2005; Bergaya *et al.*, 2006; Aguzzi *et al.*, 2007; Paul & Robeson, 2008). Applications in nanotechnology and biotechnology exploit the utility of clay minerals as nanoscale mechanical reinforcements in polymer matrices, as additives to reduce gas diffusion, and as carriers of

drug molecules related to tunable wetting and ion exchange properties. The extensive use as a filler in polymer-clay nanocomposites began with developments in the Toyota Research Laboratories in the late 1980s (Usuki *et al.*, 1993).

Extensive natural resources of clay minerals are available in geological deposits and soil that can be harvested in many parts of the world. The minerals are typically fine-grained in the micrometre range and have a layered structure with nanometre-size thickness of individual layers (Fig. 1) (Brown, 1961; Bailey, 1988). The individual layers are composed of tetrahedrally coordinated silica sheets (T) and octahedrally coordinated aluminum oxide hydroxide sheets (O) in 1:1 (TO) and 2:1 (TOT)

\* E-mail: hendrik.heinz@uakron.edu

<sup>†</sup> Presented at the Euroclay 2011 Conference at Antalya, Turkey

DOI: 10.1180/claymin.2012.047.2.05

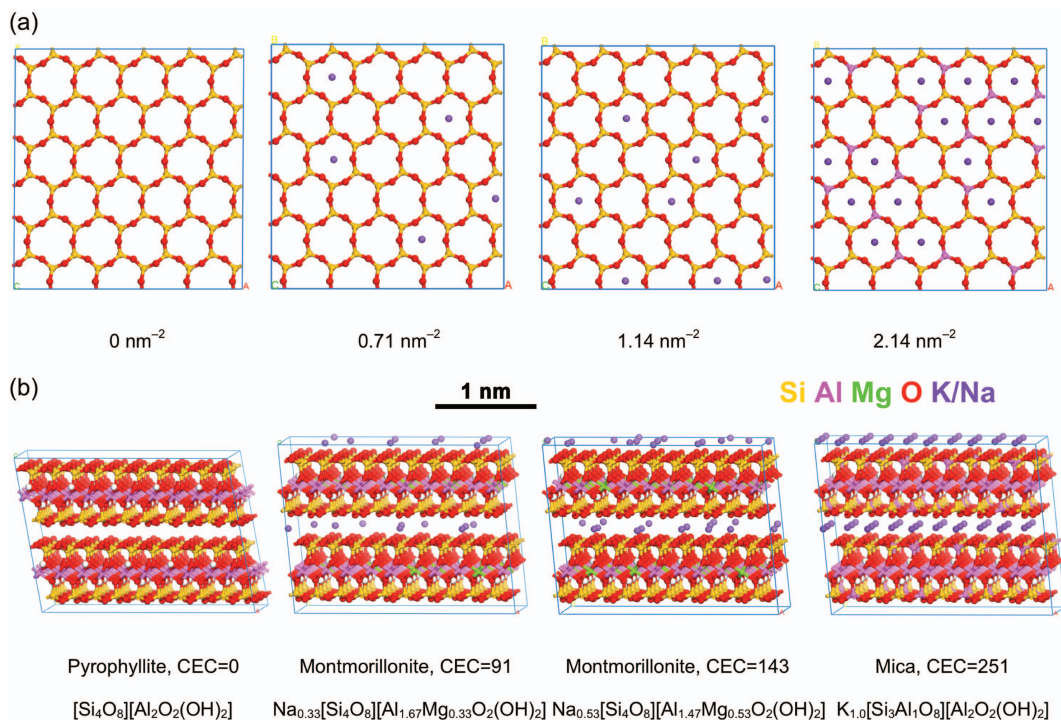


FIG. 1. Structure and chemical composition of selected 2:1 clay minerals that are widely used in nanotechnology and biotechnology (smectites, vermiculites and micas). (a) The top view depicts the variable cation density on the cleaved mineral surfaces and (b) the side view shows the nanometre-scale structure of the layers. Pyrophyllite contains no interlayer cations, montmorillonite is of intermediate cation density, and muscovite mica has the highest density of 2.14 cations per square nanometre on a cleaved surface. The cation exchange capacity (CEC) is a measure of the amount of exchangeable cations in meq/100 g. The CEC for mica is a hypothetical maximum as not all interlayer cations are exchangeable related to the cohesion between the layers (data from Rothbauer, 1971; Lee & Guggenheim, 1981; adapted from Zartman *et al.*, 2010).

sandwich structures. Anionic metal substitutions such as Si → Al and Al → Mg are commonly found in tetrahedral and octahedral layers respectively. These substitutions lead to the presence of cations between individual layers to maintain charge neutrality. Clay minerals differ in their affinity for water depending on the area density and type of cations, and can also be of different colours contingent on additional substitution of silicon and aluminum by transition metals (Fe, Cr).

The variation in chemical composition of clay minerals facilitates widely tunable interactions with water (Table 1). The affinity of clay minerals for water has been extensively studied (Mooney *et al.*, 1952a,b; Giese *et al.*, 1991; Cases *et al.*, 1992a,b, 1997; Christenson, 1993; Michot *et al.*, 1994; Berend *et al.*, 1996; Osman *et al.*, 1999; Osman

& Suter, 1999, 2000; Giese & van Oss, 2002; Yariv & Cross, 2002; Heinz *et al.*, 2003; Schoonheydt & Johnston, 2007, 2011) and can be classified as water repellent, dispersible, and hygroscopic depending on the cation density and on the enthalpy of hydration of interlayer cations. The minerals tend to be hydrophobic in the absence of cations, favour cation dissociation and swelling for an intermediate area density of monovalent cations around 1.0±0.3 per nm<sup>2</sup>, and become less hydrophilic again for high area density of cations. Interlayer cations of larger size (Cs<sup>+</sup>>Rb<sup>+</sup>>K<sup>+</sup>>Na<sup>+</sup>>Li<sup>+</sup>) reduce the enthalpy of hydration and the affinity of clay minerals to water, while smaller cations augment the enthalpy of hydration along with a higher affinity of clay minerals for water. Divalent cations (Mg<sup>2+</sup>, Ca<sup>2+</sup>) increase the cohesion between

TABLE 1. Affinity of clay minerals to water (data from Giese *et al.*, 1991; Christenson, 1993; Osman & Suter, 1999; Schoonheydt & Johnston, 2007, 2011).

Water affinity	Example	Reason
Repellant Dispersible	Pyrophyllite Mica (K <sup>+</sup> )	No surface cations, contact angle 80° High cation density, contact angle ~5°, no spontaneous delamination
Hygroscopic	Montmorillonite	Intermediate cation density, contact angle 0°, instant adsorption of vapour from air and swelling (solvation of loosely packed interlayer cations)

the mineral layers, making hydration more difficult. As an example, the hydrophilicity of montmorillonite leads to moist interlayer spaces and immediate swelling in water. Flotation of montmorillonite produces thixotropic slurry that is useful in drilling liquids to mitigate the discharge of solid parts at high drilling speed. The extraction of moisture by montmorillonite also allows uses as an additive in greases. The tunability of water retention among various clay minerals facilitates applications in paints and cosmetics, further enhanced by the natural variability in colour and glossiness related to transition metal substitution (Fe, Cr). Clay minerals are also employed in aqueous media as carriers for drug delivery, in formulations for wound healing, and as antibacterial agents (Lin *et al.*, 2002; Ray Aguzzi *et al.*, 2007). It has also been shown that hydrophobic clay minerals can

exhibit hydrophilic character at the microscopic scale (Michot *et al.*, 1994).

Layered silicates, as well as surfactant-modified layered silicates, are also used as fillers in plastics, rubber, and polymer films to increase the mechanical strength and barrier properties in comparison to neat polymers and polymer blends (Paul & Robeson, 2008) (Fig. 2). These applications rely on the nanometre-scale anisotropy and stiffness of the clay minerals, particularly the high in-plane elastic moduli of ~160 GPa (Sachse & Ruoff, 1975; Simmons & Wang, 1971; Vaughan & Guggenheim, 1986; McNeil & Grimsditch, 1993; Catti *et al.*, 1994; Habelitz *et al.*, 1997; Smyth *et al.*, 2000; Pawley *et al.*, 2002; Zartman *et al.*, 2010) in comparison to typical elastic moduli of polymers of the order of 0.1 to 1 GPa (Brandrup *et al.*, 1999) (Table 2). Applications of clay-polymer nanocom-

TABLE 2. Linear mechanical properties of clay minerals (in GPa), showing a characteristically high Young's modulus in the layer plane and small shear moduli parallel to the layer plane. Square brackets indicate approximate tensile and shear strengths. The values are experimental (Sachse & Ruoff, 1975; Simmons & Wang, 1971; Vaughan & Guggenheim, 1986; McNeil & Grimsditch, 1993; Catti *et al.*, 1994; Habelitz *et al.*, 1997; Smyth *et al.*, 2000; Pawley *et al.*, 2002) and in part consistently derived from computation (*ab initio* calculations and classical molecular dynamics; see Zartman *et al.*, 2010). In comparison, the Young's modulus of many polymers is of the order of 0.1 to 1 GPa (Brandrup *et al.*, 1999). Uncertainties are ±5%.

	Young's modulus in-plane (xx and yy)	Young's modulus (zz) at 1 GPa stress	Bulk modulus at 1 GPa stress	Shear modulus (xy)	Shear modulus (xz and yz)
Pyrophyllite (CEC 0)	160 [1, 4]	38	37	71 [1]	5 [0.2]
Montmorillonite (CEC 91)	160 [3, 4]	32	29	71 [1]	2.5 [0.25]
Montmorillonite (CEC 143)	160 [3, 20]	60	43	71 [3]	4 [0.25]
Mica (max. CEC 251)	160 [6, 20]	60	59	71 [3]	16 [1]

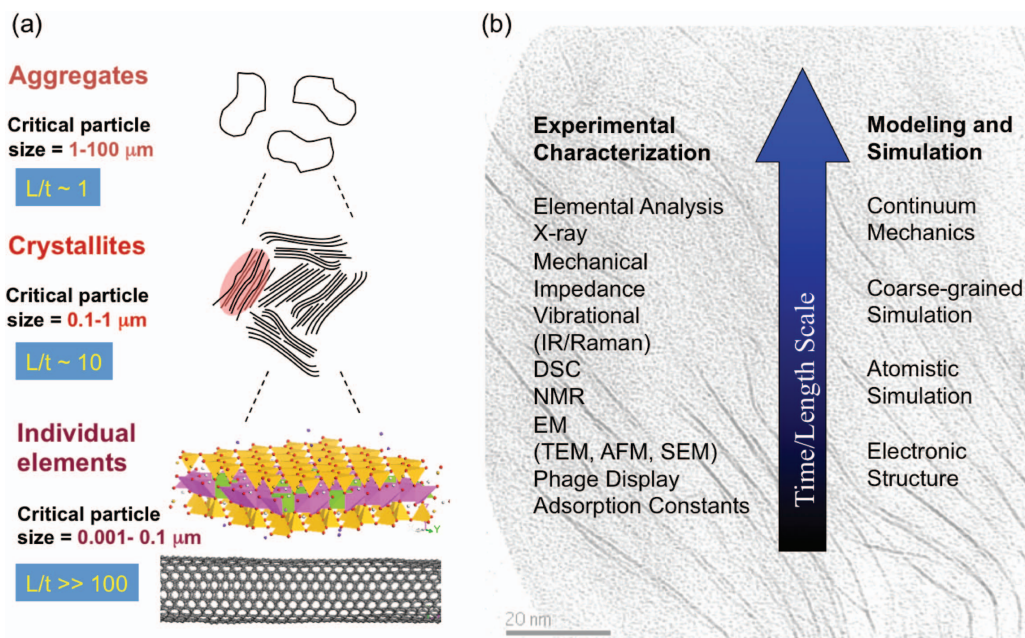


FIG. 2. (a) Aggregation state of filler materials. The aspect ratio (length over thickness) is highest for individual elements such as single aluminosilicate layers or carbon nanotubes. High aspect ratio leads to more interfacial area in an organic or biological matrix and increased mechanical stability. The directed assembly of smaller units into desired bulk morphology opens up a wider spectrum of potential properties. (b) Common techniques for the characterization of clay-polymer nanocomposites and clay-biological hybrid materials. A transmission electron micrograph of a montmorillonite-polymer nanocomposite is displayed in the background. Dispersed montmorillonite layers appear as “hairs” perpendicular to the plane (courtesy of Richard A. Vaia, AFRL).

posites involve lightweight automotive and aerospace parts to replace metals, thin films for packaging, and other commodities. The minerals are often mixed into the polymer at a weight fraction of few percent, yet high weight fractions (up to 50%) are also employed for laminates. In many instances, the polar mineral surfaces are organically modified prior to mixing to increase compatibility with hydrophobic polymers. Exfoliation of individual clay layers in the polymer matrix, rather than aggregates, is commonly desired to improve mechanical, thermal, and dielectric properties although it is often still a challenge.

For any application, control over desired morphologies at the nanometre scale is usually a challenge because experimental manipulation tools are limited and monitoring of interfaces is often impossible. For the analysis of such properties, molecular models and simulations of clay minerals and interfaces with surfactants, biomolecules and

polymers have been added to the available laboratory instrumentation (Teppen *et al.*, 1997; Heinz *et al.*, 2003, 2005; Cygan *et al.*, 2004). The utility of simulation as an integral tool for gaining insight into multi-phase materials will also be shown in the following sections.

The outline is as follows. First, nanoscale surface properties and their relation to chemical structure are reviewed, including quantitative insight into the extent of ionic bonding versus covalent bonding. Second, surface modification of clay minerals with organic surfactants, thermal transitions, and responses to light are described. This section also describes quantitative measures of exfoliation in polymer matrices and the accessible spectrum of cleavage energies. Third, tensile, shear, and bending properties are discussed, including stability limits and failure mechanisms under stress. Fourth, the mechanism of biomolecular adsorption on clay mineral surfaces is reviewed. The paper closes with a brief summary and view of future perspectives.

## NANOSCALE SURFACE PROPERTIES AND MOLECULAR MODELS

The interaction of clay minerals with water, surfactants, polymers and biomolecules is largely controlled by exchangeable cations, polar interactions, hydrogen bonds at the mineral surface, and van der Waals interactions. Laboratory measurements often provide only indirect information, so that better understanding has been achieved in conjunction with atomistic models and simulation (Fig. 2b) (Hackett *et al.*, 1998; Pospisil *et al.*, 2001, 2004; Kuppa & Manias, 2002; Heinz, 2010; Heinz & Suter, 2004a,b; Heinz *et al.*, 2003, 2004, 2005, 2006, 2007, 2008a,b; Cygan *et al.*, 2004, 2009; Zeng *et al.*, 2004; Pandey *et al.*, 2005, 2010; Greenwell *et al.*, 2005; He *et al.*, 2005; Fermeglia & Pricl, 2007; Suter & Coveney, 2009; Mazo *et al.*, 2008; Zartman *et al.*, 2010; Fu & Heinz, 2010a,b; Fu *et al.*, 2011).

The structure of dioctahedral clay minerals involves stacked layers (Fig. 1). Each layer is a triplet of sheets of silica, aluminum oxide hydroxide, and another sheet of silica that are covalently joined. The layers stack non-covalently on top of each other, and an example for this core TOT structure is pyrophyllite (Fig. 1). The presence of  $[\text{SiO}_2] \rightarrow [\text{AlO}_2^-] \text{K}^+$  substitutions in the tetrahedral outer sheets and of  $[\text{AlO}(\text{OH})] \rightarrow [\text{MgO}(\text{OH})^-] \text{Na}^+$  substitutions in the octahedral inner sheet, respectively, leads to the addition of cations such as  $\text{K}^+$  and  $\text{Na}^+$  in the spaces between the layers. Examples of these structures are montmorillonites and mica (Fig. 1). The cations are located in superficial cavities of  $[\text{Si}, \text{O}]$  rings in the tetrahedral layer, close to the sites of negative charge (Brown, 1961; Rothbauer, 1971; Lee & Guggenheim, 1981; Heinz *et al.*, 2005).

The unique properties of clay minerals are associated with the anisotropic layered structure, the polarity and the interlayer charge. Models have shown that quantitative understanding of the polarity in clay minerals is key to explaining numerous properties (Fig. 3) (Heinz & Suter, 2004b). The polarity can be represented by spatially ( $\sim$ spherically) averaged atomic charges which amount to  $+1.1 \pm 0.1e$  on Si atoms and  $-0.55e$  on O atoms ( $e$  represents units of the elementary charge) in the outer tetrahedrally coordinated silica sheets. The atomic charge on octahedral aluminum atoms amounts to  $+1.45 \pm 0.10e$  and the associated

negative charge is distributed over the coordinated O atoms. The values are supported by multiple evidence including deformation electron densities from X-ray diffraction (Hill, 1979; Ngo & Schwarzenbach, 1979; Lewis *et al.*, 1982; Belokoneva *et al.*, 2002), dipole moments of silicon compounds by laboratory measurements, an Extended Born model, and relationships to analogous compounds in the periodic table (see Heinz & Suter, 2004b). Previous computer models assumed values between  $0.5e$  and  $+4e$  on Si that have no physical significance and resulted in misleading surface properties. For example, surface tensions and cleavage energies could be up to 15 times (1500%) overestimated and excessive water ordering observed at the interface compared to experimental measurements when formal charges such as  $+4e$  on Si and  $-2e$  on O are employed in models (Table 3) (Heinz *et al.*, 2005).

In the presence of  $[\text{SiO}_2] \rightarrow [\text{AlO}_2^-] \text{K}^+$  defects and  $[\text{AlO}(\text{OH})] \rightarrow [\text{MgO}(\text{OH})^-] \text{Na}^+$  defects, the additional negative charge at the metal defect sites is distributed over the metal atom and the surrounding electronegative O atoms so that the metal atom then carries a reduced charge of about  $+0.8e$  ( $\text{AlO}_2^-$  defect) and  $+1.1e$  ( $\text{MgO}(\text{OH})^-$  defect) (Fig. 3a,b). The spatial distribution of these defect sites on the superficial tetrahedral sheet and in the inner octahedral sheet for a given stoichiometry of the mineral is known from  $^{29}\text{Si}$  and  $^{27}\text{Al}$  solid state nuclear magnetic resonance (NMR) measurements (Lipsicas *et al.*, 1984; Sanz & Serratos, 1984; Herrero & Sanz, 1991; see summary in Heinz & Suter, 2004a) and has been implemented in models (Fig. 3c,d). Direct O bridges between defect metals such as  $\text{Al}-\text{O}-\text{Al}$  or  $\text{Mg}-\text{O}-\text{Mg}$  are avoided (Loewenstein's rule) and the preferred pattern of defect sites involves some clustering, i.e. it is not fully homogeneous.

The surface structure and polarity control many properties, such as aggregation *versus* solubility of the layers, diffusion constants of cations and surfactants on the surface, adsorption equilibria of proteins, drug molecules, and humic substances in aqueous environment, as well as the orientation and morphology of self-assembled alkyl monolayers. For analysis on the nanometer scale, models for molecular simulation of clay minerals and interfaces with surfactants, biomolecules and polymers have been developed (Teppen *et al.*, 1997; Heinz *et al.*, 2003, 2005; Cygan *et al.*, 2004). The classical (non-quantum mechanical) energy expression for

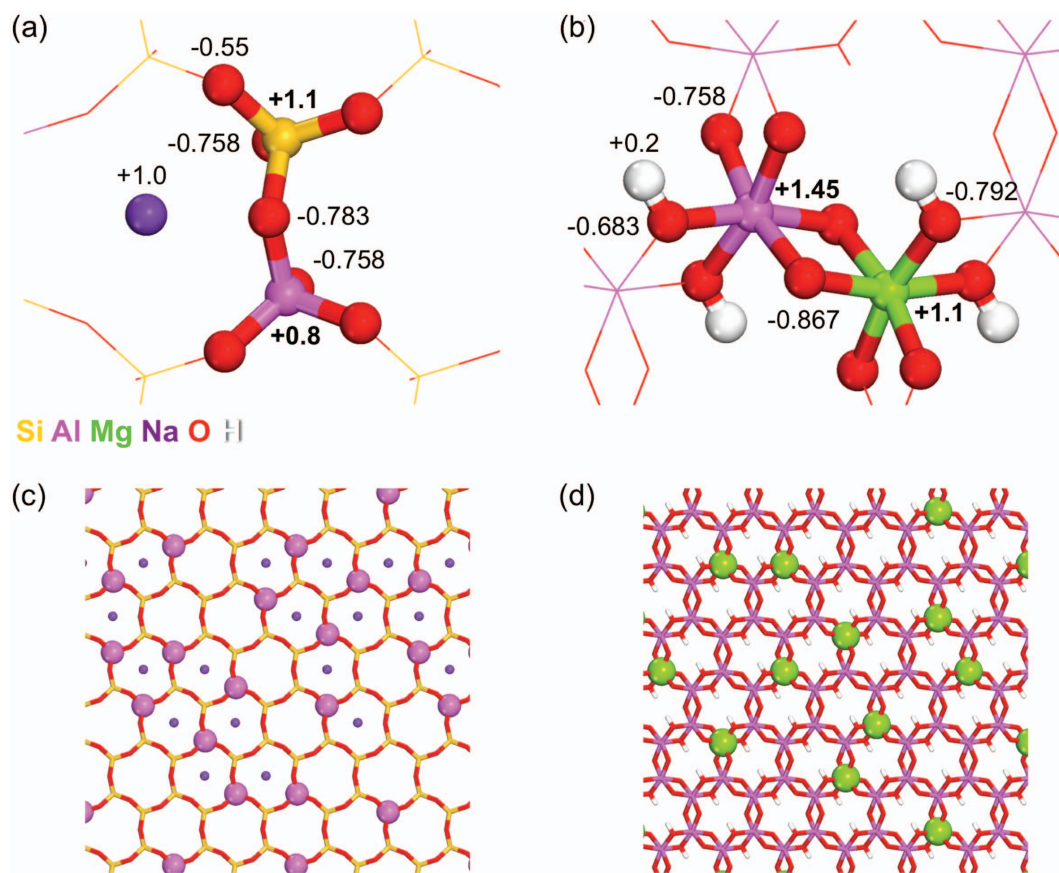


FIG. 3. (a,b) Atomic charges for the smallest structural repeat fragments in units of the elementary charge. The charges characterize the polarity of clay minerals and of anionic-cationic substitution sites. Quantitative knowledge of the extent of covalent versus ionic bonding is a key aspect for reliable simulations and understanding interfacial properties. The values are experimental (Hill, 1979; Ngo & Schwarzenbach, 1979; Lewis *et al.*, 1982; Belokoneva *et al.*, 2002) and consistent with the extended Born model (see Heinz & Suter 2004b). (a) Atomic charges in the tetrahedral sheet, including the redistribution of electron density at a  $[\text{SiO}_2] \rightarrow [\text{AlO}_2]^- \text{K}^+$  substitution site in mica (top view). The potassium ion is located in a superficial cavity. (b) Atomic charges in the octahedral sheet in units of the elementary charge, including the redistribution of electron density at a  $[\text{AlO}(\text{OH})] \rightarrow [\text{MgO}(\text{OH})]^- \text{Na}^+$  substitution site in montmorillonite (top view). The corresponding  $\text{Na}^+$  ion is located on top of the tetrahedral sheet and is not shown. (c,d) Top view onto the outer tetrahedral layer and the inner octahedral layer across a larger area ( $3.26 \times 3.26 \text{ nm}^2$ ). The spatial distribution of the anionic-cationic substitution sites is shown by large spheres in agreement with solid state  $^{29}\text{Si}$  and  $^{27}\text{Al}$  NMR data (Lipsicas *et al.*, 1984; Sanz & Serratos, 1984; Herrero & Sanz, 1991; see summary in Heinz & Suter, 2004a). (c) The spatial distribution of tetrahedral defect sites (Al) in mica and (d) of octahedral defect sites (Mg) in montmorillonite (CEC 91 meq/100 g). A certain local association of defects is seen as opposed to a fully homogeneous distribution.

atomistic models typically includes terms for quadratic bond stretching, quadratic angle bending, Coulomb interactions and van der Waals energy. The phyllosilicate force field (PFF) (Heinz *et al.*, 2005) yields computed cell parameters of clay

minerals in about 0.5% agreement with X-ray data (Lee & Guggenheim, 1981; Rothbauer, 1971) (Fig. 1), and computed surface tensions and cleavage energies in about 5% agreement with experimental measurements (Chassin *et al.*, 1986;

TABLE 3. Reliability of force fields for the simulation of interfaces of clay minerals with water, polymers, and biological molecules. The phyllosilicate force field (PFF, Heinz *et al.*, 2005) yields surface tensions ( $\gamma^{\text{tot}} = \gamma^{\text{el}} + \gamma^{\text{vdW}}$ ) and cleavage energies in vacuum ( $\Delta E_c$ ) in quantitative agreement with laboratory measurements (data from Chassin *et al.*, 1986; Adams & Gast, 1997; Giese & van Oss, 2002). Earlier force fields including CLAYFF (Cygan *et al.*, 2004) deviate from physically justified charges and van der Waals parameters, leading to large deviations in computed surface properties.

	Surface tension			Cleavage energy		Atomic charges ( <i>e</i> )		VdW param/Well depths (kcal/mol)		
	Pyrophyllite $\gamma^{\text{tot}}$	$\gamma^{\text{el}}$	$\gamma^{\text{vdW}}$	Montm. $\Delta E_c$ (MJ/m <sup>2</sup> )	Mica	Si <sup>tet</sup>	Al <sup>oct</sup>	Si	Al	O
Expt	39.7	5.8	33.9	50–200	375	1.2	1.45	–	–	–
Sim PFF	40	8	32	140	380	1.1	1.45	0.03	0.03	0.015
Sim CLAYFF	81	30	51	167	484	2.1	1.58	10 <sup>-6</sup>	10 <sup>-6</sup>	0.155
Sim OTHER	-1094	+2	-1107	-3000	-433	0.52	1.33	0	0	0
	to	to	to	to	to	to	to	to	to	to
	+265	+155	+252	+340	+683	4.0	3.0	0.40	9.04	6.86

Adams & Gast, 1997; Giese & van Oss, 2002) (Table 3). The quantitative evaluation of atomic charges for Coulomb interactions and of van der Waals parameters enables the reproduction of electrostatic and van der Waals contributions to the surface tension of pyrophyllite (Giese & van Oss, 2002). Thermodynamic consistency of the phyllosilicate energy expression with biological and materials oriented force fields (PCFF, CVFF, CHARMM, AMBER) facilitates the simulation of mineral-organic and aqueous mineral interfaces for durations of nanoseconds to microseconds at a length scale of 1 to 100 nm (up to approximately one million atoms). Shortcomings in experimental and theoretical validation of other computer models can lead to significantly higher deviations from measurements, such as up to 5% in cell parameters compared to X-ray data and up to 500% in surface energies (Teppen *et al.*, 1997; Greathouse *et al.*, 2000; Kuppa & Manias, 2002; Cygan *et al.*, 2004; Mazo *et al.*, 2008).

Using the PFF models, it is possible to analyse the composition of the surface and cleavage energies of montmorillonite and mica (Fig. 4). Cohesion between the layers in the natural minerals is clearly dominated by Coulomb contributions (Fig. 4a). Surface modification by organic surfactants leads to the separation of surface cations before cleavage occurs and reduces the cleavage energy by nearly an order of magnitude (Heinz *et al.*, 2006) (Fig. 4b). Then, in essence, only van der Waals interactions remain between the layers.

## SURFACE MODIFICATION AND RESPONSES TO HEAT AND LIGHT

### *Overview of surfactant self-assembly, packing density, and the inorganic-organic interface*

Some polymers for nanocomposites are soluble in water and can be mixed with hydrophilic clay minerals, e.g. montmorillonite, without surface modification. Such polymers are, for example, polyethylene oxide, polyacrylic acid, chitosan and hyaluronic acid. Most polymers for automotive, aerospace and packaging applications, however, are hydrophobic and require aluminosilicate layers with hydrophobic surfaces to achieve exfoliation and dispersion. Examples of such polymers are polyethylene, polypropylene, polystyrene, polymethylmethacrylate (PMMA), bisphenol-A polycarbonate, epoxy resins, polyurethanes, polyimides, nylon-6 and aramides. Therefore, organic surface modification of clay minerals plays an important role in achieving miscibility with hydrophobic polymer matrices (Fig. 4). The properties of organically modified clay surfaces also affect the nanoscale structure and micrometre-scale morphology of clay-polymer nanocomposites, and thus the desired mechanical, gas permeation and thermal properties.

Modification of clay minerals by cation exchange with amphiphilic surfactants has been known for a long time and is well understood today (Weiss *et al.*, 1956; Gaines, 1957; Lagaly & Weiss, 1970, 1971; Breen *et al.*, 1997; Osman & Suter, 1999, 2000; Osman *et al.*, 1999, 2000, 2002, 2004; Bergaya & Lagaly, 2001; Heinz *et al.*, 2003,

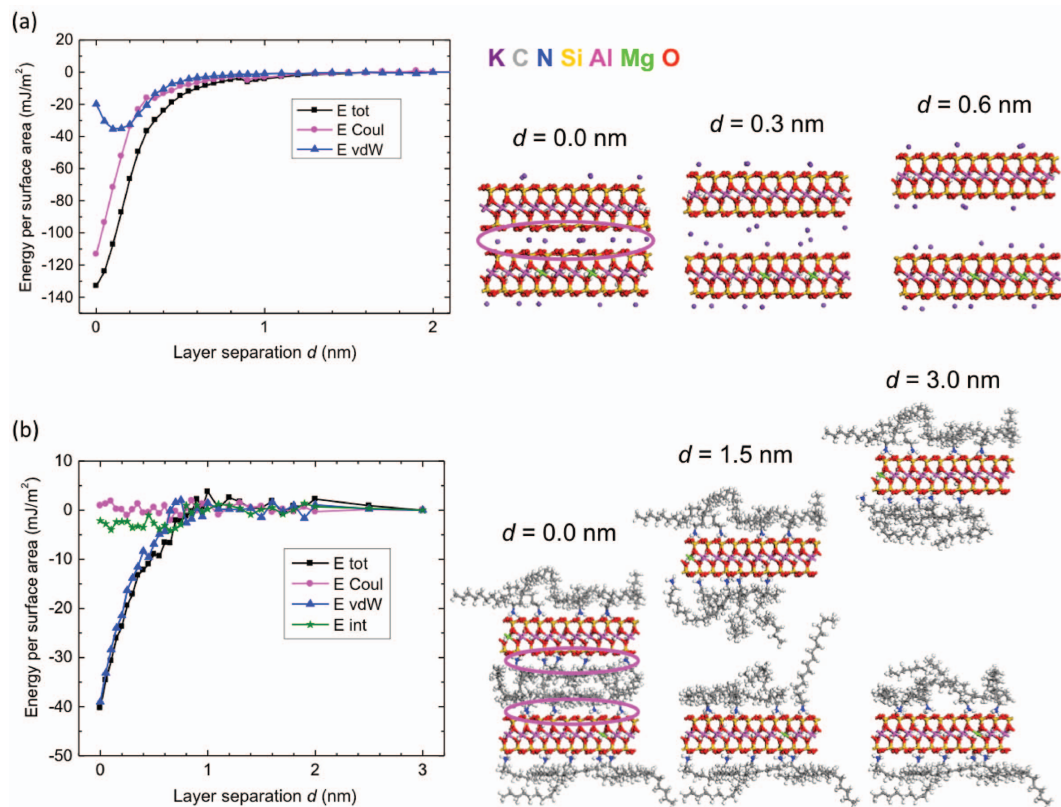


FIG. 4. Cleavage energy of sodium montmorillonite and shielding of Coulomb forces by the alkyl chains in the interlayer of octadecylammonium montmorillonite. (a) The cleavage energy of the unmodified mineral is predominantly composed of Coulomb energy to afford the distribution of the alkali cations between the two layers, which occurs at short distances below 0.5 nm layer separation. (b) The cleavage energy of the modified mineral is reduced by  $\sim 70\%$  due to the separation of the head groups pertaining to each of the two layers before cleavage by the  $\sim 0.8$  nm thick organic layer (see oval highlights). Entropic contributions to the cleavage free energy are negligible in the natural clay minerals and typically low for organically modified clay minerals (smaller than  $-5$  mJ m<sup>-2</sup>), related to conformational changes of the alkyl chains. For the unmodified and for the modified mineral, no significant forces ( $< 3$  mJ m<sup>-2</sup>) are felt beyond the 2–3 nm separation of the layers (adapted from Heinz *et al.*, 2006).

2005, 2007). To achieve the conversion of the polar and often hydrophilic surfaces of clay minerals into less polar and hydrophobic surfaces, ion exchange reactions often involve alkylammonium or alkylphosphonium halides in aqueous and alcoholic solution. The surfactants replace alkali cations on the mineral surface through the ammonium head groups. After washing and solvent removal, the alkyl tails of the surfactants aggregate as horizontal alkyl layers, tilted alkyl layers, or nearly perpendicular alkyl layers on the mineral surface, depending on the cation density, extent of ion exchange and length of the alkyl chains (Fig. 5) (Weiss *et al.*,

1956; Lagaly, 1976; Lagaly & Weiss, 1970, 1971; Vaia *et al.*, 1994; Hayes & Schwartz, 1998; Brovelli *et al.*, 1999; Pospisil *et al.*, 2001, 2004; Zeng *et al.*, 2004; Heinz & Suter, 2004a; Heinz *et al.*, 2003, 2004, 2005, 2006, 2007, 2008a,b; He *et al.*, 2005; Greenwell *et al.*, 2005).

A useful order parameter for the observed surface structure and dynamics of organically modified clay minerals is the packing density  $\lambda_0$  of the alkyl chains, which equals the ratio between the cross-sectional area of an extended alkyl chain  $A_{C,0}$  and the available surface area per cation  $A_S$  (Heinz *et al.*, 2003, 2008a). The packing density is controlled

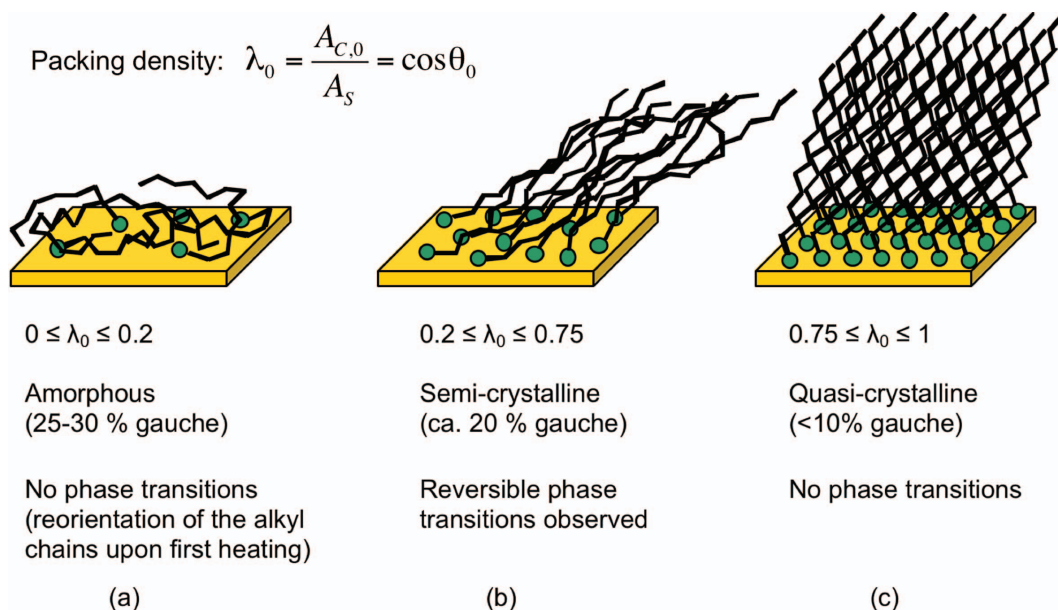


FIG. 5. Range of structures and thermal properties of homogeneous alkyl layers on even surfaces of clay minerals (as well as on oxidic, metallic and other surfaces). The packing density  $\lambda_0$  is a useful order parameter, defined as the cross-sectional area of a fully extended alkyl chain  $A_{C,0}$  divided by the available surface area per chain  $A_S$  (a) At low packing density, alkyl chains are conformationally disordered and oriented nearly horizontal to the surface. (b) At intermediate packing density, intermediate tilt angles and intermediate conformational order of the backbones are found, and reversible melting transitions upon heating occur. (c) At high packing density, well ordered, near perpendicular alkyl monolayers are formed. The self-assembled patterns can be explained by optimization of van der Waals interactions between individual alkyl chains. The packing density determines the average segmental tilt angle of the alkyl chains relative to the surface normal  $\theta_0$ . Order-disorder transitions upon heating occur at intermediate packing density as a result of increased thermal motion of the alkyl backbones and lateral mobility of the surfactant head groups on the surface (adapted from Heinz *et al.*, 2008a).

by the surfactant geometry, i.e. number of alkyl chains per head group, and by the cation density of the surface, i.e. the known CEC of a clay mineral (Fig. 1). In cases of non-stoichiometric cation exchange, island formation of the alkyl chains on the surface has also been observed (Hayes & Schwartz, 1998; Osman *et al.*, 2002; Heinz & Suter, 2004a). In homogeneous portions of the modified surface, the packing density ranges between 0 and 1 whereby flat-on layers correspond to lowest packing densities between 0.0 and 0.2, intermediately tilted layers to packing densities between 0.2 and 0.75, and well ordered, nearly perpendicular monolayers to packing densities between 0.75 and 1.0 (Fig. 5).

The type of surfactant head group also influences the structure of the inorganic-organic interface (Fig. 6) (Heinz *et al.*, 2005, 2007). Primary ammonium ions are located closer to superficial

cavities in comparison to quaternary ammonium ions due to the formation of up to three hydrogen bonds. Coulomb forces between the head group and the layer are, therefore, strongly shielded by primary ammonium groups (Fu & Heinz, 2010a,b). The nitrogen atom in quaternary ammonium groups is, in contrast, located more than twice as far from the surface compared to the nitrogen atom in primary ammonium groups, which leads to more conformational flexibility, ease of lateral diffusion, and significantly less shielding of Coulomb forces between the surfactant and the mineral. The strength of surface-head group interaction affects lateral diffusion of the surfactants on the surface, thermal transitions and cleavage energies, while the influence on the structure of the alkyl monolayer and on the gallery spacing is small.

Modification of the clay mineral surface with surfactants can also introduce new chemical

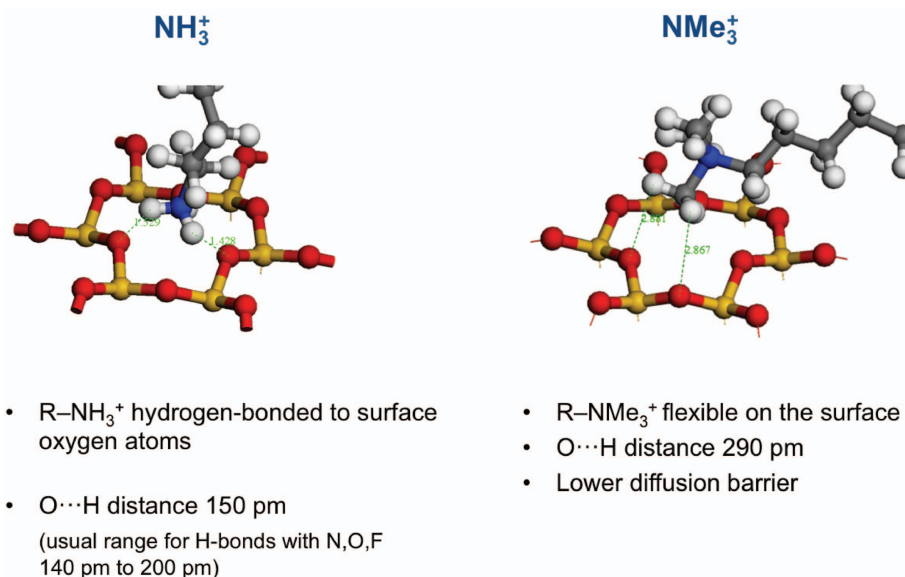


FIG. 6. Differences between head groups at the aluminosilicate-surfactant interface. The closest O···H distance is shorter for hydrogen-bonded primary ammonium groups ( $\text{Si}_2\text{O}\cdots\text{H}-\text{N}$ ) than for non-hydrogen-bonded quaternary ammonium groups ( $\text{Si}_2\text{O}\cdots\text{H}-\text{C}$ ), leading to stronger adsorption and lower mobility on the surface (adapted from Heinz *et al.*, 2007).

functionality. For example, superficial alkylammonium surfactants containing additional alcohol or amine groups enable cross-linking reactions of the modified clay minerals with epoxy precursors for the *in situ* preparation of clay-epoxy thermoplastic nanocomposites. In the following we will systematically discuss the structure, dynamics and interfacial properties of organically modified clay minerals.

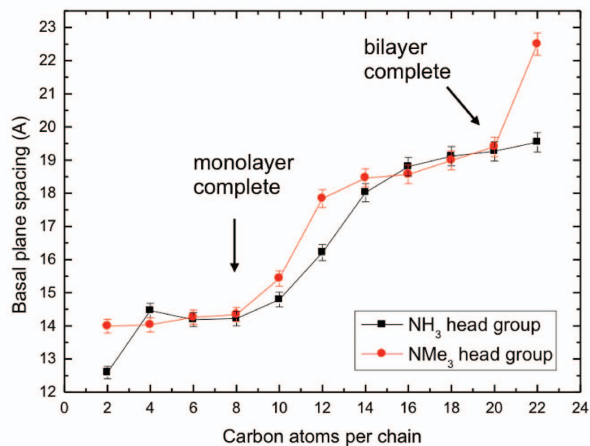
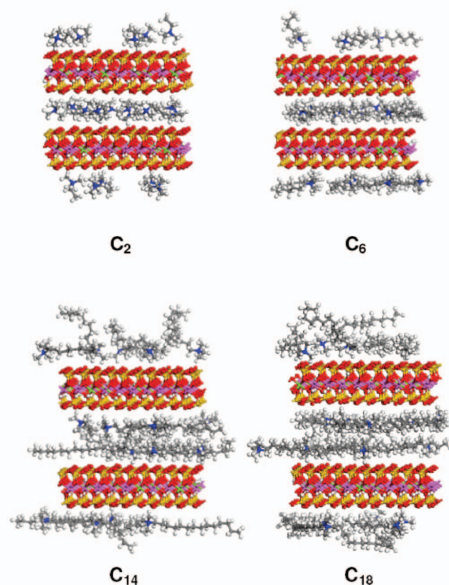
*Alkylammonium-modified layered silicates at low packing density: interlayer structure, chain conformation, cleavage energy, and exfoliation in nanocomposites*

The packing density  $\lambda_0$  of single-chain surfactants on montmorillonites and other smectites is low. The reason is the cross-sectional area of a single alkyl chain of  $A_{C,0} = 0.188 \text{ nm}^2$  and the low number density of cations per surface area, for example  $1/A_S = 0.71 \text{ nm}^{-2}$  and  $1/A_S = 1.14 \text{ nm}^{-2}$  for montmorillonite of CECs of 91 and 143 meq/100 g, respectively. The resulting packing density of 0.13 to 0.21 for *n*-alkylammonium ions (or *n*-alkyltrimethylammonium ions) on montmorillonite leads to the arrangement of flat-on alkyl layers in the interlayer space (Fig. 5). The basal plane

spacing and the interlayer thickness increase stepwise as the length of the alkyl chains increases (Fig. 7). The assembly of a loosely packed horizontal alkyl monolayer, a densely packed alkyl monolayer, a partial alkyl bilayer, a densely packed alkyl bilayer, and so forth upon increase in chain length has been observed in X-ray diffraction and by molecular simulation (Table 4). The layering effect decreases beyond trilayers and quadrilayers due to the conformational flexibility of the alkyl chains (Lagaly & Weiss, 1971; Vaia *et al.*, 1994, 1997; Osman *et al.*, 2004, 2005; Lagaly & Dekany, 2005; Heinz *et al.*, 2007, 2008b).

The nonlinear plateau-and-step increase in basal plane spacing as a function of chain length leads to fluctuations in the interlayer density of the alkyl chains and in backbone conformations, represented by the percentage of gauche conformations (Fig. 8). For example, the observation of nearly constant basal plane spacing for a range of increasing chain lengths of the surfactants from C<sub>14</sub> to C<sub>20</sub> for CEC 91 meq/100 g (Fig. 7a) causes an increase in interlayer density. The interlayer density is thus low in the presence of a partially packed horizontal alkyl monolayer and increases toward high interlayer density for a densely packed alkyl monolayer, followed by a drop in interlayer density upon

(a) CEC = 91 meq/100 g,  $N(CH_3)_3^+-(CH_2)_n-H$



(b) CEC 143 meq/100 g,  $NH_3^+-(CH_2)_n-H$

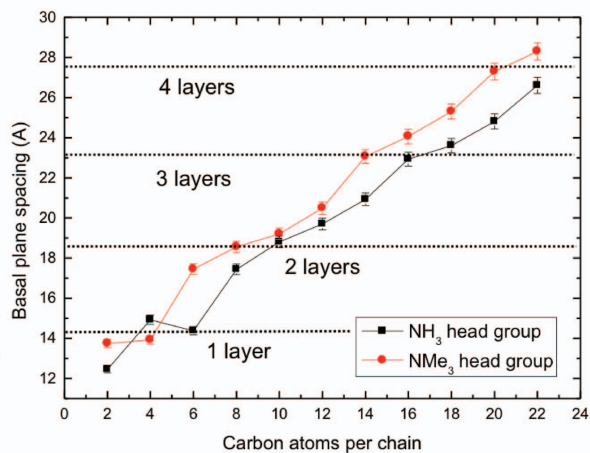
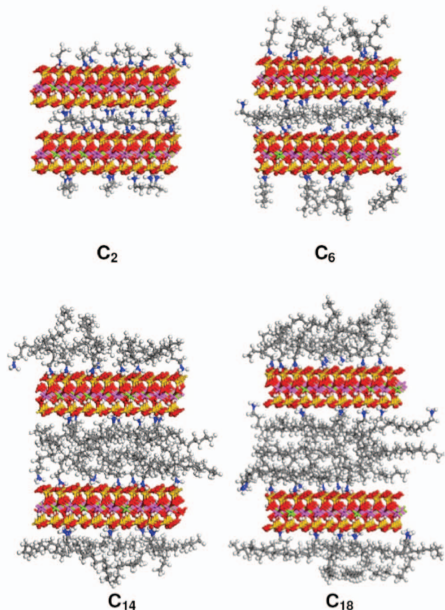


FIG. 7. Basal plane spacing and interlayer structure of *n*-alkylammonium montmorillonites as a function of chain length at low packing density. (a) CEC 91 meq/100 g, packing density  $\lambda_0 = 0.13$ . (b) CEC 143 meq/100 g, packing density  $\lambda_0 = 0.21$ . The flat-on orientation of the alkyl chains and successive layer-by-layer “filling” of the interlayer space as a function of chain length can be seen. The plateau-and-step progression of the thickness of the alkyl layers is more pronounced at lower packing density (a) as the segmental tilt angle of the alkyl chains relative to the surface normal is then nearer to  $90^\circ$  (adapted from Heinz *et al.*, 2007; Fu & Heinz, 2010b).

TABLE 4. The basal plane (nm) spacing of alkylammonium montmorillonites of different charge ( $\mu\text{eq}/100\text{ g}$ ) according to X-ray data (Lagaly & Weiss, 1971; Vaia & Giannelis, 1997; Vaia *et al.*, 1997; Osman *et al.*, 2004, 2005; Lagaly & Dekany, 2005; Heinz *et al.*, 2007) and atomistic simulation (Heinz *et al.*, 2007). The agreement is very good and differences of the order of 5% are related to uncertainties in mineral composition and homogeneity (experimental) as well as limitations in the molecular models (simulation).

	— $\text{H}_3\text{NR}^+/\text{CEC} = 91$ —		— $\text{H}_3\text{NR}^+/\text{CEC} = 145$ —	
	Expt	Sim.	Expt.	Sim.
C <sub>4</sub>	1.36 (3)	1.45 (2)		
C <sub>6</sub>	1.36 (3)	1.42 (2)	1.50 (3)	1.44 (2)
C <sub>8</sub>	1.36 (3)	1.42 (2)		
C <sub>10</sub>	1.45 (3)	1.48 (3)	1.80 (3)	1.89 (3)
C <sub>12</sub>	1.70 (3)	1.62 (3)	1.87 (3)	1.97 (3)
C <sub>14</sub>	1.75 (3)	1.80 (3)	2.03 (3)	2.09 (3)
C <sub>16</sub>	1.75 (3)	1.88 (3)	2.28 (3)	2.29 (3)
C <sub>18</sub>	1.85 (2)	1.91 (3)	2.30 (3)	2.36 (3)
Std. dev. to expt.		0.08 (5%)		0.08 (5%)

formation of a partially packed horizontal alkyl bilayer (Fig. 8a). The low-density interlayer space in loosely packed alkyl layers easily attracts solvent molecules or  $\text{CO}_2$  from air unless the organically modified clay minerals are kept under low pressure or vacuum.

Assuming dry clay minerals, the variation in interlayer packing and in interlayer density as a function of chain length causes differences in the conformation of the alkyl chains (Fig. 8b). A lower interlayer density allows the alkyl chains to assume a higher percentage of energetically favourable anti-conformations since more lateral interlayer space is available. A higher interlayer density enforces a higher fraction of gauche conformations because the alkyl chains pack more densely and assume energetically less favourable chain rotations. In this manner, van der Waals contacts are optimized and lower basal plane spacing is maintained unless the chains are longer, so that an additional, loosely packed alkyl layer is formed (Heinz *et al.*, 2007).

The binding of head groups to the surface (Fig. 6) exerts an additional influence on chain conformations. Primary ammonium head groups  $\text{H}_3\text{N}^+-\text{R}$  are smaller than quaternary head groups  $(\text{CH}_3)_3\text{N}^+-\text{R}$  and located in the cavities of  $[\text{Si}, \text{O}]$  12-rings in the tetrahedral layer close to negatively charged metal substitution sites. H atoms of the primary ammonium head groups form up to three hydrogen bonds with superficial O atoms in the tetrahedral layer, leading to a tripod-like position on the surface (Fig. 6). This position of primary

alkylammonium ions on the clay mineral surface increases the amount of gauche conformations of the C–C bond near the N-terminus which is reflected in an increased percentage of gauche conformations at short chain lengths (Fig. 8b). In contrast, larger and non-hydrogen bonding trimethylalkylammonium head groups have orientational freedom on the surface (Fig. 6), higher lateral mobility, and do not impose additional gauche conformations (Fig. 8b). The head-group dependent and chain-length dependent amount of gauche conformations is supported by infrared (IR) and nuclear magnetic resonance (NMR) measurements, i.e. by shifts in the symmetric and asymmetric  $\text{CH}_2$  stretching frequencies as well as by  $^{13}\text{C}$  spectral shifts (Vaia *et al.*, 1994; Osman *et al.*, 2000, 2002, 2004; Zhu *et al.*, 2005; Jacobs *et al.*, 2006; see Heinz, 2007).

Differences in the interlayer environment further lead to variations in the cleavage energy of organically modified layered silicates (Figs 4 and 9) (Heinz *et al.*, 2006; Fu & Heinz, 2010a,b). The cleavage energy is high for short chains of alkyltrimethylammonium ions (Fig. 9a,b) because bulky quaternary ammonium groups reside in the middle of the interlayer and lead to very strong Coulomb interactions (Fig. 9c), similar to alkali cations in montmorillonite (Fig. 4a). The cleavage energy is low for short chains of primary alkylammonium ions (Fig. 9a,b) because the head groups are pre-separated between the two layers, so that only marginal Coulomb forces must be

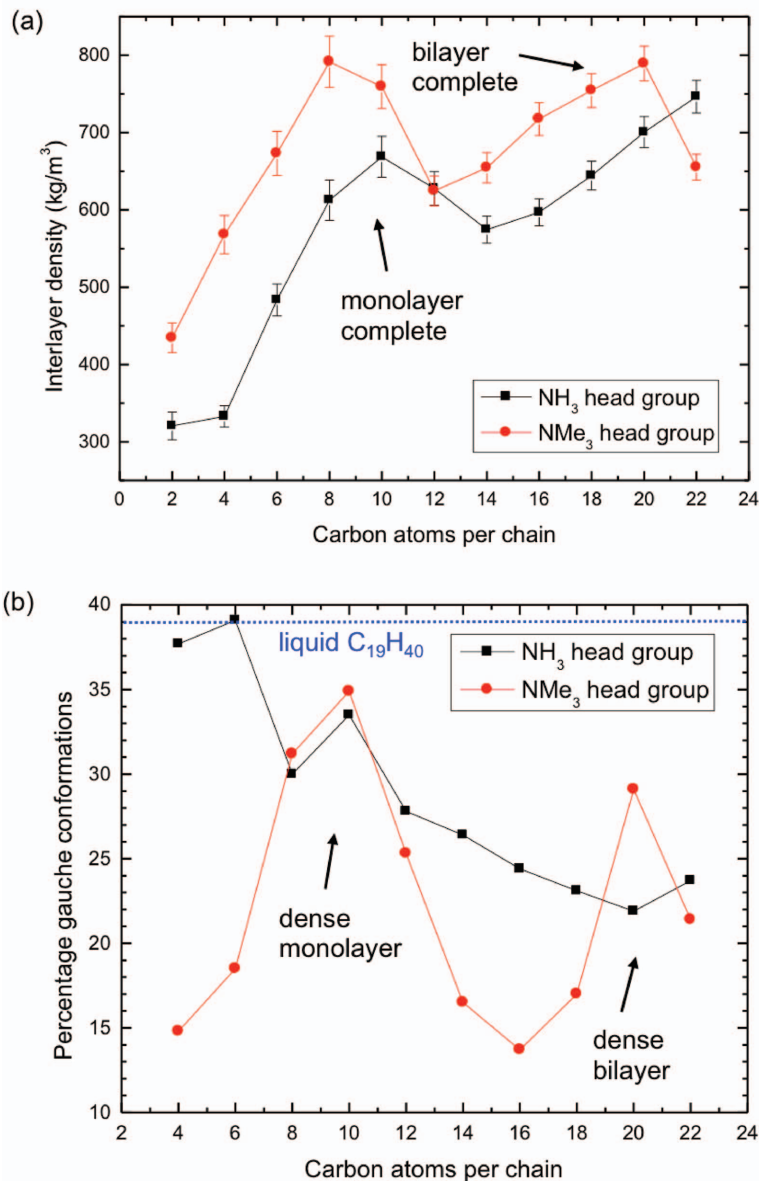
CEC = 91 meq/100 g,  $N(CH_3)_3^+- (CH_2)_n-H$ 

FIG. 8. (a) Interlayer density and (b) percentage of gauche conformations of the alkyl chains in *n*-alkylammonium montmorillonite of CEC 91 meq/100 g as a function of head group chemistry and chain length ( $\lambda_0 = 0.13$ ). The percentage of gauche conformations in liquid nonadecane is shown for comparison. The alkyl chains on the montmorillonite surface have a lower percentage of gauche conformations and can be considered between solid and liquid state (adapted from Heinz *et al.*, 2007).

overcome to separate the layers (Fig. 9c), similar to alkylammonium montmorillonite with longer alkyl chains (Fig. 4b). In addition to these electrostatic

effects, the cleavage energy depends on the strength of van der Waals interactions between the modified clay layers as a function of chain length. Lower

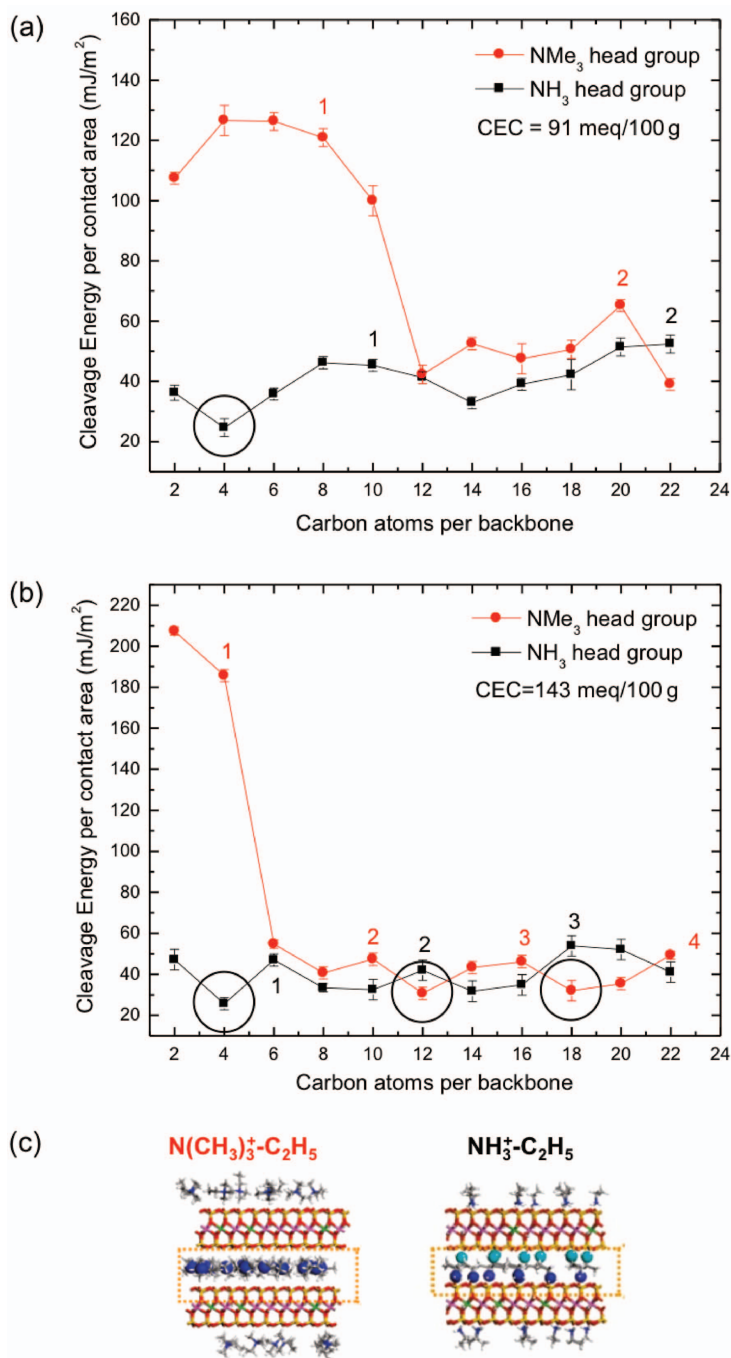


FIG. 9. Cleavage energy of alkylammonium montmorillonites as a function of CEC, head group, and chain length. (a) CEC 91 meq/100 g, (b) CEC 143 meq/100 g, (c) short quaternary versus short primary ammonium surfactants at CEC 143 meq/100 g. Shielding of Coulomb interactions and low interlayer density can lead to minimal cleavage energies (circled highlights) up to  $15 \text{ mJ m}^{-2}$  lower than surface tensions of the cleaved and reconstructed surfaces. Integer labels 1, 2, 3 on the graphs indicate the formation of densely packed alkyl monolayers, bilayers and trilayers respectively (adapted from Fu & Heinz, 2010a).

interlayer density and loose packing of alkyl chains decrease the cleavage energy (circular highlights in Fig. 9a,b). Densely packed interlayers with higher interlayer density increase the cleavage energy. In summary, the cleavage energy of alkylammonium-modified montmorillonites depends on electrostatic interactions and on packing of the surfactant chains. The lowest cleavage energy was identified for butylammonium montmorillonites as  $25 \text{ mJ m}^{-2}$  (circular highlights in Fig. 9a,b). We note that these data rely on computational models (Heinz *et al.*, 2005) as experimental instrumentation is not available to perform equivalent measurements. The confidence in simulation results is high, however, as the computation of related properties (basal plane spacing, interlayer density, chain conformations and surface tensions) shows quantitative agreement with experiment (Heinz *et al.*, 2005, 2006, 2007; Fu & Heinz, 2010a,b).

Cleavage energies make a contribution to exfoliation and dispersion of modified layered silicates in polymer matrices (Fig. 10). The free energy balance of dispersion of mineral layers in polymer matrices  $\Delta G$  has three contributions (Fig. 10a,b). These are the cleavage of the mineral layers  $\Delta G_M$ , the creation of void spaces in the polymer  $\Delta G_P$ , and the formation of the mineral-polymer interface  $\Delta G_{MP}$ . One possibility to lower  $\Delta G$  and improve exfoliation consists in lowering the cleavage energies to less than surface tensions by choice of a specific clay mineral and a specific surfactant. This is possible because cleavage free energies  $\Delta G_M$  differ from surface tensions  $\gamma_M$  (Fig. 10c). For example, the cleavage energy of mica is  $375 \text{ mJ m}^{-2}$  and the surface tension is  $\sim 60 \text{ mJ m}^{-2}$  (Christenson, 1993; Adams & Gast, 1997). For organically modified montmorillonites, cleavage energies range from 25 to  $210 \text{ mJ m}^{-2}$  (Fu & Heinz, 2010a) while surface tensions range from 40 to  $45 \text{ mJ m}^{-2}$  (Giese & van Oss, 2002; Lewin *et al.*, 2005; Kamal *et al.*, 2009). Cleavage energies measure a separation process of the layers including surface reconstruction while surface tensions measure the free energy of a static, already cleaved surface in contact with liquids. To achieve exfoliation in nanocomposites, the cleavage free energy  $\Delta G_M$  is relevant and not the surface tension (Fig. 10d,e) (Fu & Heinz, 2010a). The other contributions  $\Delta G_P$  and  $\Delta G_{MP}$  to the cleavage free energy  $\Delta G$  are not significantly affected by changes in the type of surfactant grafted to the clay mineral surface. Any surfactant creates similar void spaces in the polymer ( $\Delta G_P$ ) and polymer interactions with the

cleaved surfaces ( $\Delta G_{MP}$ ) scale with the surface tension of the cleaved mineral surface, not with the cleavage energy.

Therefore, the minimization of cleavage energies ( $\Delta G_M \sim \epsilon_S$ ) by choice of a suitable combination of clay mineral and surfactant is a possible pathway to improve exfoliation of organically modified clay minerals in polymer matrices (Fu & Heinz, 2010a). This concept, however, still requires practical tests. Limitations might arise due to very high  $\Delta G_P$  in the presence of entangled polymer chains, or due to thermal decomposition of the alkylammonium-modified clay minerals during melt processing of the polymer-clay mixture at temperatures exceeding  $300^\circ\text{C}$  (Osman *et al.*, 2004). An increase in thermal decomposition temperature may be achieved by using alkylammonium surfactants that lack H atoms in  $\beta$  positions, which hinder the Hofmann elimination mechanism (Heinz *et al.*, 2003).

#### *Alkylammonium-modified layered silicates at intermediate and high packing density: interlayer dynamics and thermal transitions*

The packing density of surfactants on clay minerals can be increased using surfactants composed of multiple alkyl chains or clay minerals of greater cation density. For example, dialkylammonium or trialkylammonium surfactants, instead of monoalkylammonium surfactants, will double or triple the packing density respectively. The use of montmorillonite of a higher CEC or of mica will also increase the packing density relative to smectites of lower CEC. When the packing density exceeds 0.2, the formation of increasingly tilted alkyl layers is observed rather than the formation of horizontal alkyl layers (Fig. 5). Periodic fluctuations in interlayer structure, density, and chain conformations as a function of chain length are not found (Fig. 11), although reversible melting transitions of the alkyl chains emerge at intermediate packing densities (Fig. 11a). The transition from horizontally layered structures to near-vertical layers can be followed by comparison of Fig. 7a ( $\lambda_0 = 0.13$ ), Fig. 7b ( $\lambda_0 = 0.21$ ), Fig. 11a ( $\lambda_0 = 0.40$ ) and Fig. 11b ( $\lambda_0 = 0.80$ ). At high cation densities, when the ion exchange reaction was carried out substoichiometric, it is also possible that the surface contains spatially separate domains of alkali ions and of tilted alkyl chains (see AFM data by Hayes & Schwartz, 1998; comparison of basal plane spacing with simulation results by Heinz & Suter, 2004a).

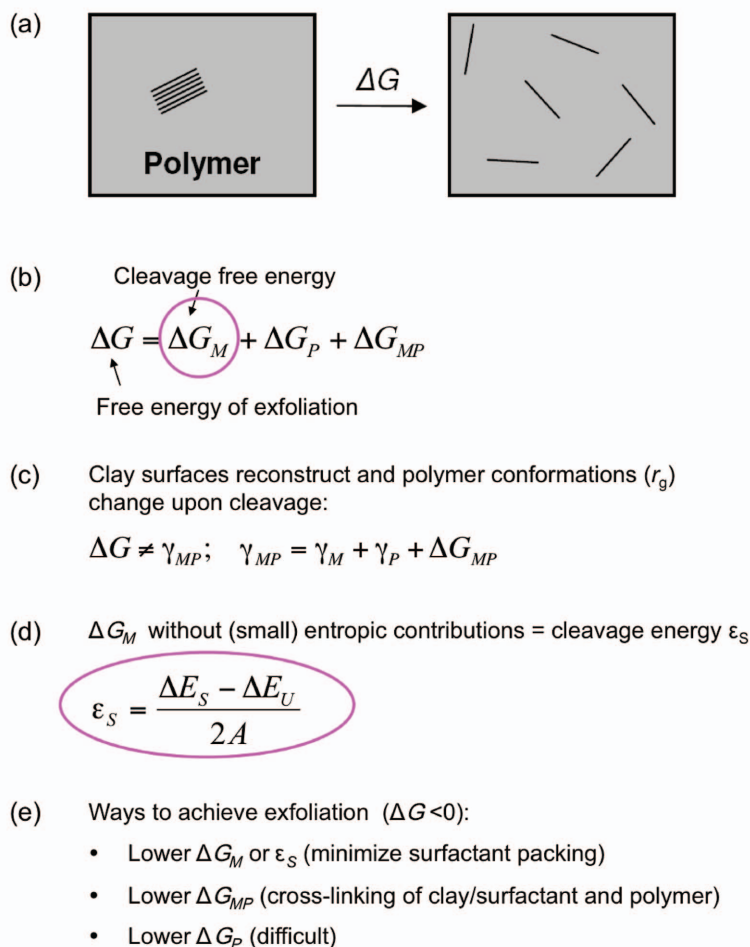


FIG. 10. (a) Schematic diagram of homogeneous distribution (exfoliation) of layered silicates in a polymer matrix and the associated balance of free energy. (b) The free energy of exfoliation  $\Delta G$  involves contributions by the cleavage of the mineral layers  $\Delta G_M$ , creation of void spaces in the polymer  $\Delta G_P$ , and recombination of the cleaved mineral surface with the polymer  $\Delta G_{MP}$ . (c) The surfaces of clay minerals and polymers change their structure in this process so that the free energy of exfoliation  $\Delta G$  cannot be expressed as an interface tension  $\gamma_{MP}$ . (d) Cleavage free energies of clay minerals  $\Delta G_M$  can be approximated by cleavage energies  $\epsilon_S$ , i.e. the difference in energy in the separated and unified state over the contact area. The cleavage energies are tunable over a wide range using different surfactants without significant changes in the surface tension of cleaved minerals  $\gamma_M$  and in the mineral-polymer free energy of interaction  $\Delta G_{MP}$ . (e) Exfoliation can thus be driven by lower cleavage energies  $\Delta G_M$  or by cross-linking between filler and matrix (lower  $\Delta G_{MP}$ ). The free energy for void creation in the polymer  $\Delta G_P$  is more difficult to tune as it may require another polymer, and such changes could be offset by  $\Delta G_{MP}$  (adapted from Fu & Heinz, 2010a).

The packing density is uniquely determined by the cation density of the mineral and the surfactant composition, and is suitable for describing the structure, tilt angle and thermal transitions of homogeneous alkyl layers (Fig. 12) supported by a wide range of data (see Heinz *et al.*, 2008a).

An intermediate degree of order of the alkyl chains at intermediate packing density leads to the occurrence of reversible phase transitions upon heating (Fig. 11a). In a typical temperature range from  $-20^\circ\text{C}$  to  $100^\circ\text{C}$ , one or two phase transitions have been observed by differential scanning

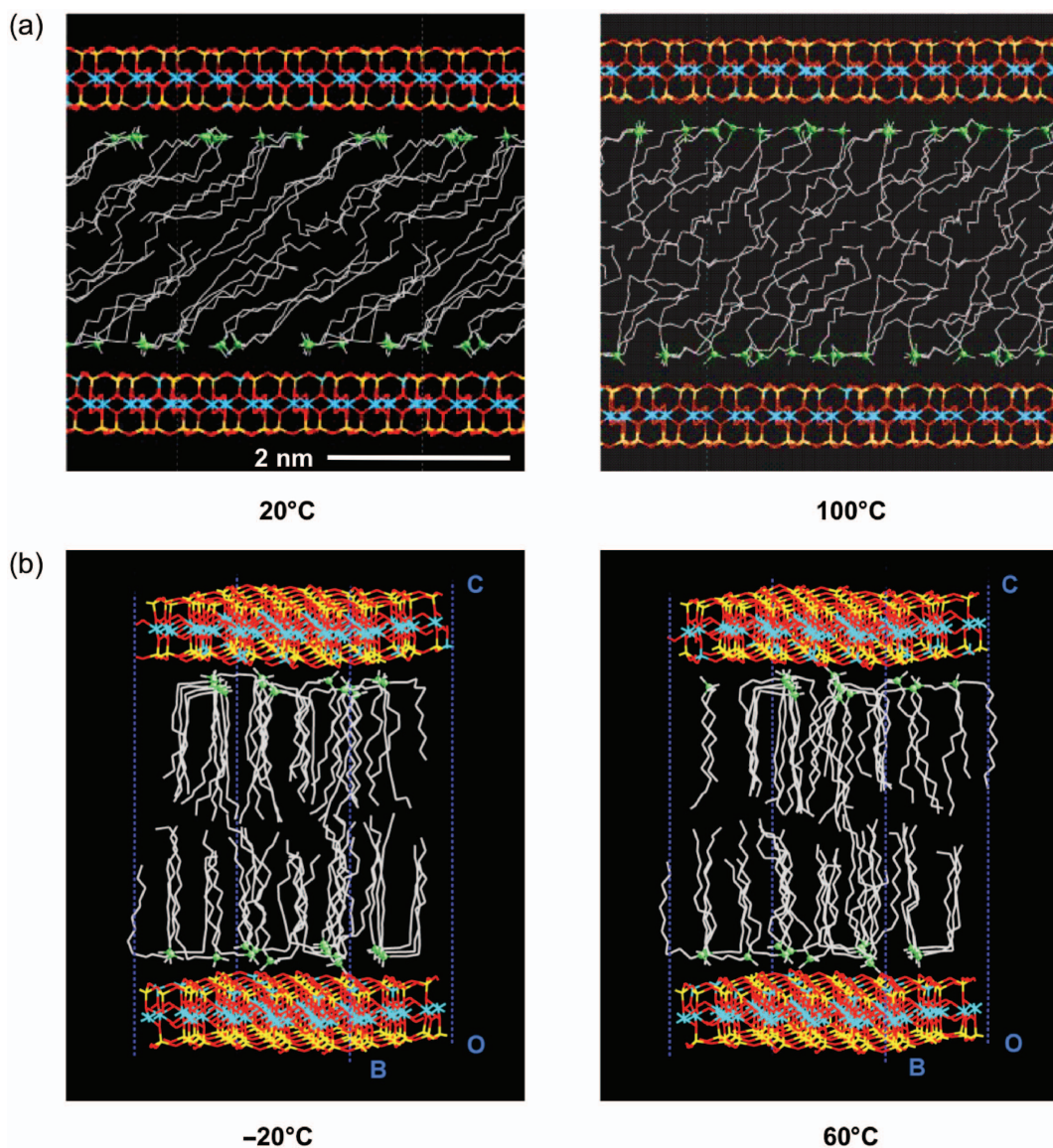


FIG. 11. (a) Structure of octadecyltrimethylammonium ions on mica, packing density  $\lambda_0 = 0.40$  at 20°C and at 100°C. A reversible melting transition upon heating is observed by DSC (Osman *et al.*, 2000) and in the simulation (Heinz *et al.*, 2003) in which the percentage of gauche conformations changes from 24% to 31%. (b) Structure of didodecyldimethylammonium ions on mica, packing density  $\lambda_0 = 0.80$  at -20°C and at 60°C. No melting transition is seen upon heating in DSC (Osman *et al.*, 2002) and in the simulation. The percentage of gauche conformations changes from 9% to 12% (Heinz & Suter, 2004a).

calorimetry (DSC) (Osman *et al.*, 2000, 2002, 2004). One possible transition involves lateral rearrangements of quaternary ammonium head groups on the surface and a second transition involves reversible “melting” of the tethered alkyl

chains from disordered rods to broken rods (Heinz *et al.*, 2003). The first transition is exclusive for surface-mobile quaternary ammonium surfactants and does not occur with primary ammonium surfactants due to strong surface bonding (Fig. 6).

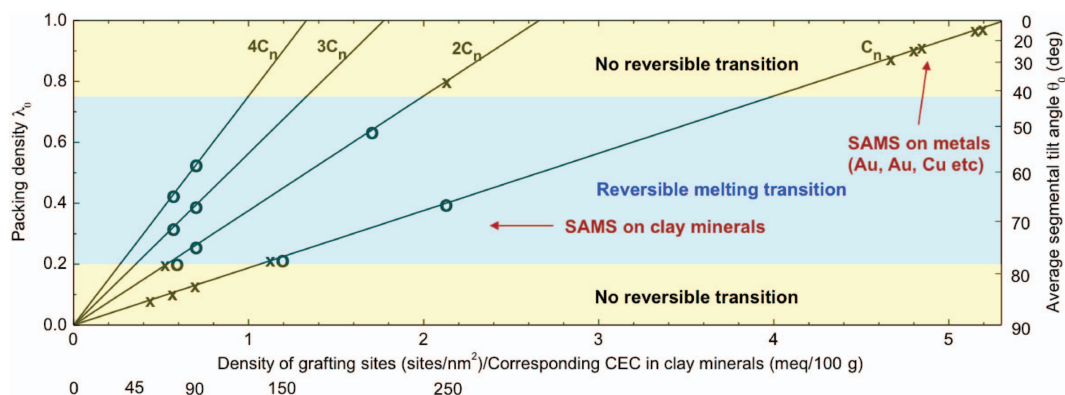


FIG. 12. Diagram of packing density, tilt angle and thermal behaviour for a given combination of surfactant and surface. The four straight lines indicate the packing density of monoalkylammonium, dialkylammonium, trialkylammonium and tetraalkylammonium surfactants on a clay mineral surface of known cation density (grafting density) or CEC respectively. The occurrence (O) or absence (X) of reversible melting transitions on heating is indicated for data points from laboratory measurements. The prediction also holds for other oxide and metal surfaces, assuming a homogenous distribution of surfactant molecules and a minimum chain length  $\geq C_{10}$  (from Heinz *et al.*, 2008a).

Upon cooling to room temperature, this transition is only observable again after a few hours relaxation time as the reverse lateral movements of the head groups are associated with significant energy barriers (estimated  $>10 \text{ kcal mol}^{-1}$ ). The second transition, which involves partial melting of the tethered alkyl chains, is immediately reversible and not dependent on the type of head group.

When the packing density is high, i.e. above 0.75, the percentage of gauche conformations diminishes and the dense packing of surfactants leads to negligible “melting” effects (Figs 5c and 11b). No thermal transitions occur in DSC (Osman *et al.*, 2002, 2004) and only a modest increase in the fraction of gauche conformations is seen that decreases the effective tilt angle  $\theta$  relative to  $\theta_0 = \cos\lambda_0$  in the simulation (Heinz & Suter, 2004a; Heinz *et al.*, 2004) (Fig. 11b).

In summary, at intermediate and at high packing density, no major changes in interlayer density, in conformation of the alkyl chains, and in cleavage energy are found when the chain length of the surfactants increases (except for an increase in the temperature for the order-disorder transition). The indifference of the interlayer structure to the length of the alkyl chains at medium and high packing density is opposite to the variety of packing modes as a function of chain length at low packing density. The cleavage energy of alkylammonium modified montmorillonites and micas at inter-

mediate and high packing density are in the range  $40 \text{ to } 45 \text{ mJ m}^{-2}$  (Heinz *et al.*, 2006), similar to the surface tension (Giese & van Oss, 2002; Yariv & Cross, 2002). Therefore, modification of the cleavage energy by surfactant design is not feasible as at low packing density (Figs 9 and 10). An alternative to modulate the surface structure can be sub-stoichiometric ion exchange (Hayes & Schwartz, 1998; Heinz & Suter, 2004a).

#### *Diffusion and light-induced switching on the surface*

The surfactants are bound to the surface by ionic forces and have the possibility of lateral diffusion. Surface diffusion necessitates the simultaneous motion of at least two surfactants at the same time as the head groups attempt to remain close to negatively charged surface sites (Heinz *et al.*, 2007). Surface diffusion constants depend on the head group, chain length and packing density. Quaternary ammonium head groups are more mobile than primary ammonium head groups due to the absence of hydrogen bonds with the surface (Fig. 6). Shorter alkyl chains lead to more mobility than longer alkyl chains due to weaker van der Waals interactions with neighbor chains that slow down lateral mobility. Also, a CEC of the mineral at the lower end promotes surface diffusion because steric hindrance between individual surfactants is

small. Therefore, short quaternary ammonium surfactants (tetramethylammonium) on an isolated surface at low packing density (CEC 91 meq/100 g) exhibit the highest diffusion rate ( $10^{-5}$  to  $10^{-6}$  cm<sup>2</sup> s<sup>-1</sup>), about one order of magnitude less than the self-diffusion constant of water. The equivalent primary ammonium surfactants show diffusion constants at least two orders of magnitude lower, and the presence of longer chains, as well as higher packing density further reduces diffusion constants by several orders of magnitude (no quantitative values known; Heinz *et al.*, 2007).

The ability to form layered structures of well defined basal plane spacing has also led to studies that attempt reversible optical switching of the basal plane spacing. Studies using X-ray diffraction, UV/VIS spectroscopy, and simulation have shown modest reversible switching between 5 and 10% in montmorillonites modified with azobenzene-containing surfactants (Iyi *et al.*, 2001; Ogawa *et al.*, 2001, 2003; Okada *et al.*, 2005; Heinz *et al.*, 2008b). Upon laser irradiation at ~420 nm, the surfactants can flip from the *cis* to the *trans* conformation and cause an expansion of the interlayer space. Upon irradiation at ~365 nm, the *trans* conformation switches to the *cis* conformation and causes a contraction of the interlayer space. A challenge to achieve more than 2–5% reversible switching, however, is the compensation of the change in interlayer density. The surfactants need to be designed to be rigid and grafted perpendicular to the surface to generate a 10% reversible actuation in basal plane spacing. The response time can be very fast.

Alternatively, co-intercalates such as phenol can be used to reversibly enter into the gallery space and exit the gallery space to compensate changes in interlayer density upon optical switching. Phenol solvates *cis*-azobenzene better than *trans*-azobenzene due to a higher dipole moment, thus leading to larger basal plane spacing for the *cis* isomer, not the *trans*-isomer. The amount of optical switching in gallery height can then exceed 40%; however, reported increases are not uniform and the response time is much longer (Okada *et al.*, 2005).

## TENSILE, SHEAR AND BENDING PROPERTIES

2:1 clay minerals are anisotropic and have a high in-plane stiffness of 160 GPa (Table 2). The in-plane stiffness does not depend on CEC and applied

stress, and is a major reason for the utility of clay minerals as a mechanical reinforcement in composites. The stiffness perpendicular to the layers is lower and depends both on the CEC and on the applied stress. The perpendicular modulus is about 60–80% lower than the in-plane modulus at 1 GPa applied stress, and increases toward the in-plane modulus for higher applied stress (up to 20 GPa) for all CECs (Zartman *et al.*, 2010). The softest mineral in the series of increasing CEC is montmorillonite of low CEC (91 meq/100 g) where a *zz* modulus (perpendicular to the layer) of only ~6 GPa was reported at a low applied stress of 10 MPa (Vanorio *et al.*, 2003). Clay minerals also exhibit low shear stability parallel to the layers. Unmodified clay minerals often fail by sliding of the layers, and the shear stability is particularly low in the presence of organic surface modification. Shear moduli of natural clay minerals parallel to the layers (in *xz* and *yz* direction) are 2 to 16 GPa and the shear strength before onset of shear flow is 0.2 to 1.0 GPa depending on the CEC (Table 2) (Zartman *et al.*, 2010).

A common observation is also bending of layered silicates (Fig. 13). Bending of individual layers requires comparatively minor energies. The necessary mechanical energy per layer area to achieve a radius of curvature from infinity to 20 nm is of the order of 10 mJ m<sup>-2</sup> or less according to simulation and observations in composites (Fu *et al.*, 2011) (Fig. 13a,b). For stronger deformations down to 6 nm radius of curvature, the elastically stored energy per layer area quickly reaches several hundred mJ m<sup>-2</sup> and the corresponding energy density exceeds that of ultracapacitors (Fig. 13b). Investigation of the bending mechanism by molecular models has shown that the deformation of bond angles and bond lengths accounts for the majority of the bending energy and that the radius of curvature may reach very small values before failure (Sato *et al.*, 2001; Fu *et al.*, 2011) (Fig. 13c,d). The dissociation of chemical bonds may require up to 10<sup>4</sup> mJ m<sup>-2</sup> so that single layers and agglomerates have considerable resistance against failure when slowly deformed. The smallest observed radius of curvature by transmission electron microscopy (TEM) is 3 nm (Fig. 13a).

At volume fractions of clay minerals in nanocomposites in the low percent range, bending radii remain typically above 100 nm. A significant fraction of highly curved layers below 20 nm radius appears for volume fractions over 5% and after

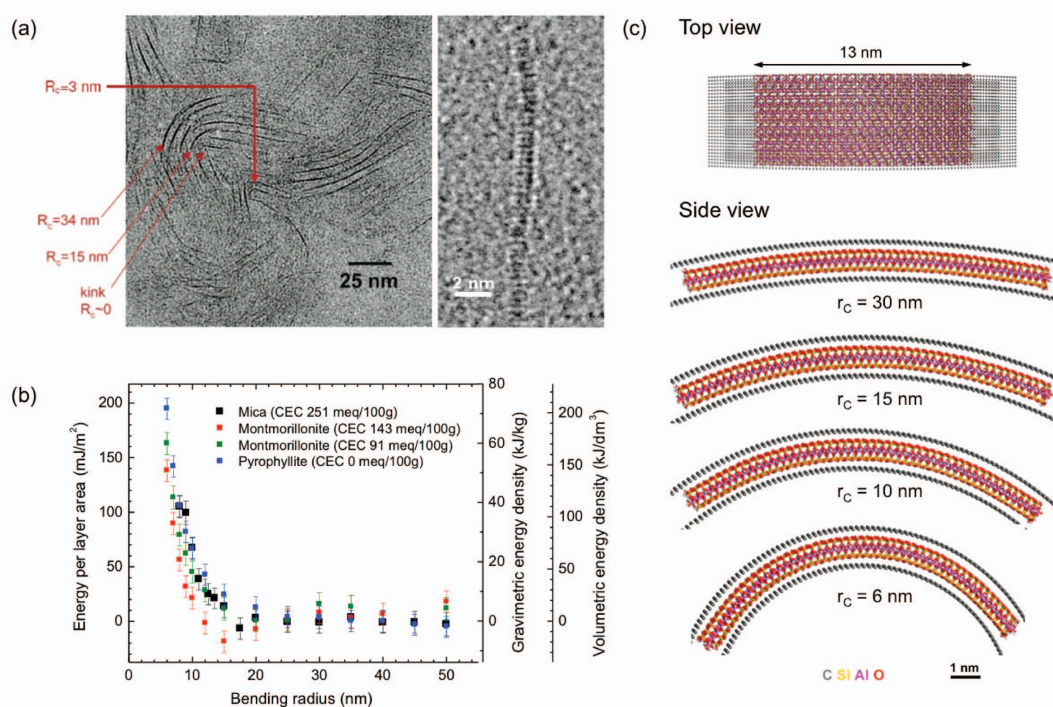


FIG. 13. Bending stability of layered silicates. (a) The smallest observed curvature by TEM is a bending radius of  $\sim 3$  nm in a montmorillonite-epoxy resin. (b) Computed bending energy per layer area as a function of bending radius for single aluminosilicate layers. The bending energy per layer area becomes significant for radii of curvature below 20 nm and exceeds (as a very minimum)  $200 \text{ mJ m}^{-2}$  before failure. (c) Models to analyse the bending energy and deformation of single layers as a function of bending radius by molecular dynamics simulation, shown for pyrophyllite. A fixed enclosure of carbon atoms of defined bending radius was used to modify and control the bending radius (from Fu *et al.*, 2011).

extrusion. Failure of layered silicates by bending involves a kink and split mechanism, and a typical reduction to half the original average length can often be observed as a result of melt processing of composites by extrusion (Fu *et al.*, 2011).

Force constants of single layers upon deformation with AFM tips were found to be in a range of  $0.15$  to  $0.4 \text{ N m}^{-1}$  (Kunz *et al.*, 2009), similar to graphene and consistent with simulation results. The force constant does not show a significant dependence on the CEC.

#### SURFACE ADSORPTION OF BIOMOLECULES

The aqueous interface of clay minerals with dissociated alkali cations provides a unique space of tunable ionic strength for the interaction with polar and charged molecules such as proteins,

carbohydrates, and drug molecules (Fig. 14) (Parbhakar *et al.*, 2007; Drummy *et al.*, 2009, 2010; Patwardhan *et al.*, 2012). By variation of CEC, cation type, pH and temperature, clay minerals can serve as substrates to bind and release a variety of biomolecules. As an example, phage display techniques have been used to identify phage-attached peptides that remain bound to the montmorillonite surface after several washing cycles in aqueous solution. Phages are thin viral capsids of approximately  $1 \mu\text{m}$  length and display cilia at the end that terminate with genetically modifiable peptides of 7–12 amino acids in length. Using a library of more than one billion phages, the peptides S2 and CR31 were identified as strongest binders to montmorillonite (Fig. 14a). The peptide of strongest identified interaction, peptide S2, contains two positive charges in the Lys side chains and is attracted to the surface at  $\text{pH} = 7$

(a)

Peptide	Sequence	pI
S2	[His <sup>+</sup> -Gly-Ile-Asn-Thr-Thr-Lys <sup>+</sup> -Pro-Phe-Lys <sup>+</sup> -Ser-Val] <sup>2+</sup> · 2 Cl <sup>-</sup>	10
CR31	Trp <sup>+</sup> -Pro-Ser-Ser-Tyr-Leu-Ser-Pro-Ile-Pro-Tyr-Ser <sup>-</sup>	5.5

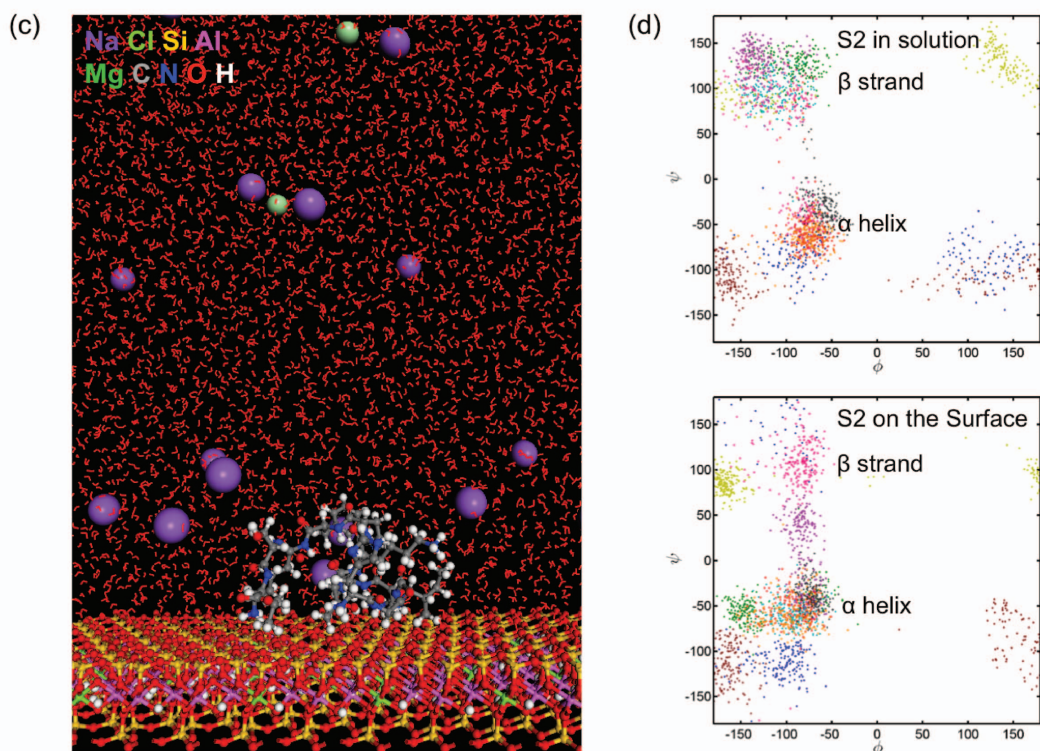


FIG. 14. (a) Peptides attracted to montmorillonite (CEC 91 meq/100 g) using phage display. Peptide S2 contains two cationic Lys side chains and is a very strong binder that can hardly be removed by washing cycles at pH = 7 (Drummy *et al.*, 2010). (b) Adsorption of the peptide S2 involves a cation exchange mechanism supported by the high isoelectric point (pI) and molecular simulation. Adsorption of nonionic peptides such as CR31 involves hydrogen bonds (Ser, Tyr) and polar interactions with the negatively charged surface. (c) Snapshot of the aqueous interface of montmorillonite with bound peptide S2 in atomistic simulation. Many sodium ions dissociate several nanometres away from the montmorillonite surface, consistent with swelling properties. The peptide replaces sodium ions near the surface and the formation of two  $Na^+ \cdots Cl^-$  ion pairs in the upper portion of the image can be seen. (Simulations involved montmorillonite (CEC 91 meq/100 g), 4000 water molecules, one peptide molecule, and the CVFF-PFF force field for 10 ns.) (d) Ramachandran plots for peptide S2 indicate  $\alpha$  helical and  $\beta$  strand conformational features in solution and on the surface, whereby the amount of helix and random coil dominate on the surface. The plot is specific for this peptide with multiple surface-binding groups.

by ion exchange (Fig. 14b). Another peptide, CR31, does not contain cationic groups and is attracted to the surface by coordination of alkali ions and hydrogen bonds (Drummy *et al.*, 2010).

The ion exchange reaction of peptide S2 can also be followed by molecular dynamics simulation and then the detachment of sodium chloride as a result of the ion exchange reaction is seen (Fig. 14c) (Heinz, 2010). Ramachandran plots suggest that the peptide conformation changes from the solution state to the adsorbed state on the surface with a slight decrease in  $\beta$  strand conformation in favour of more random coil and  $\alpha$  helical conformations (Fig. 14d). The changes in conformation are sequence-specific and may not be generalized.

This example shows that clay minerals can function as carrier and delivery substrates for molecules with biological activity, such as proteins for improved wound healing and drug molecules for controlled release (Aguzzi *et al.*, 2007). Clay minerals of low to intermediate cation density also have an anti-bacterial effect due to the high local ionic strength and fluid-absorbent properties. A wide range of target molecules can also be bound to the montmorillonite surface by covalent attachment to montmorillonite-specific peptide recognition tags (Drummy *et al.*, 2010).

## CONCLUSIONS

We have discussed a wide range of nanoscale surface properties of clay minerals which play a role for applications in composites and as carrier materials for biomolecules. The interfacial structure and polarity, the packing density of surfactants, molecular conformations, cleavage energies, aqueous interfaces, as well as responses to thermal and mechanical stimuli illustrate the rich chemistry and physics that provide the basis for the versatility and future potential of layered silicates for various technologies.

## ACKNOWLEDGMENTS

The author acknowledges support by the National Science Foundation (DMR-0955071), the Air Force Research Laboratory, AFOSR, UES Inc., Sika Technology AG, ETH Zurich, Procter and Gamble, Goodyear Tire and Rubber Company, and the University of Akron. The author gratefully acknowledges the invitation to the Euroclay 2011 Conference and support by the Euroclay Conference and the Clay Minerals Group of the Mineralogical Society.

## REFERENCES

- Adams A.W. & Gast A.P. (1997) *Physical Chemistry of Surfaces*, 6th edition. Wiley, New York.
- Aguzzi C., Cerezo P., Viseras C. & Caramella C. (2007) Use of clays as drug delivery systems: Possibilities and limitations. *Applied Clay Science*, **36**, 22–36.
- Bailey S.W. (1988) *Hydrous Phyllosilicates (Exclusive of Micas)*, *Reviews in Mineralogy*, **13**. Mineralogical Society of America, Washington D.C.
- Belokoneva E.L., Gubina Yu.K., Forsyth J.B. & Brown P.J. (2002) The charge-density distribution, its multipole refinement and the antiferromagnetic structure of diopside,  $\text{Cu}_6[\text{Si}_6\text{O}_{18}]\cdot 6\text{H}_2\text{O}$ . *Physics and Chemistry of Minerals*, **29**, 430–438.
- Berend I., Cases J.M., Francois M., Uriot J.P., Michot L., Masion A. & Thomas F. (1996) Mechanism of adsorption and desorption of water vapor by homoionic montmorillonites: 2. The  $\text{Li}^+$ ,  $\text{Na}^+$ ,  $\text{K}^+$ ,  $\text{Rb}^+$  and  $\text{Cs}^+$ -exchanged forms. *Clays and Clay Minerals*, **43**, 324–336.
- Bergaya F. & Lagaly G. (2001) Surface modification of clay minerals. *Applied Clay Science*, **19**, 1–3.
- Bergaya F., Theng, B.K.G. & Lagaly G. (2006) *Handbook of Clay Science*. Elsevier, Amsterdam.
- Brandrup J., Immergut E.H. & Grulke E.A., editors (1999) *Polymer Handbook*. Wiley, New York.
- Breen C., Watson R., Madejova J., Komadel P. & Klapayta Z. (1997) Acid-activated organoclays: Preparation, characterization and catalytic activity of acid-treated tetraalkylammonium-exchanged smectites. *Langmuir*, **13**, 6473–6479.
- Brovelli D., Caseri W.R. & Hahner G. (1999) Self-assembled monolayers of alkylammonium ions on mica: Direct determination of the orientation of the alkyl chains. *Journal of Colloid and Interface Science*, **216**, 418–423.
- Brown G. (1961) *The X-ray Identification and Crystal Structures of Clay Minerals*. Mineralogical Society, London.
- Cases J.M., Berend I., Besson G., Francois M., Uriot J.P., Thomas F. & Poirier J.E. (1992a) Mechanism of adsorption and desorption of water vapor by homoionic montmorillonite. 1. The sodium-exchanged form. *Langmuir*, **8**, 2730–2739.
- Cases J.M., Pons C.H., Berend I., Francois M., Min J.H., Tchoubar D., Besson G., Thomas F. & Bottero J. Y. (1992b) Fluid-swelling clays interaction. *Proceedings of the 6<sup>th</sup> IFP Exploration and Production Research Conference*, Institut Français du Pétrole, 27–32.
- Cases J.M., Berend I., Francois M., Uriot J.P., Michot L.J. & Thomas F. (1997) Mechanism of adsorption and desorption of water vapor by homoionic montmorillonite. 3. The  $\text{Mg}^{2+}$ ,  $\text{Ca}^{2+}$ ,  $\text{Sr}^{2+}$  and  $\text{Ba}^{2+}$  exchanged forms. *Clays and Clay Minerals*, **45**, 8–22.

- Catti M., Ferraris G., Hull S. & Pavese A. (1994) Powder neutron diffraction study of 2M<sub>1</sub> muscovite at room pressure and at 2 GPa. *European Journal of Mineralogy*, **6**, 171–178.
- Chassin P., Jounay C. & Quiquampoix H. (1986) Measurement of the surface free energy of calcium-montmorillonite. *Clay Minerals*, **21**, 899–907.
- Christenson H.K. (1993) Adhesion and surface energy of mica in air and water. *The Journal of Physical Chemistry*, **97**, 12034–12041.
- Cygan R.T., Liang J.J. & Kalinichev A.G. (2004) Molecular models of hydroxide, oxyhydroxide, and clay phases and the development of a general force field. *The Journal of Physical Chemistry B*, **108**, 1255–1266.
- Cygan R.T., Greathouse J.A., Heinz H. & Kalinichev A.G. (2009) Molecular models and simulations of layered materials. *Journal of Materials Chemistry*, **19**, 2470–2481.
- Drummy L.F., Koerner H., Phillips D.M., McAuliffe J.C., Kumar M., Farmer B.L., Vaia R.A. & Naik R.R. (2009) Repeat sequence proteins as matrices for nanocomposites. *Materials Science Engineering C*, **29**, 1266–1272.
- Drummy L.F., Jones S.E., Pandey R.B., Farmer B.L., Vaia R.A. & Naik R.R. (2010) Bioassembled layered silicate-metal nanoparticle hybrids. *ACS Applied Materials & Interfaces*, **2**, 1492–1498.
- Fermeglia M. & Pricl S. (2007) Multiscale modeling for polymer systems of industrial interest. *Progress in Organic Coatings*, **58**, 187–199.
- Fu Y.T. & Heinz H. (2010a) Cleavage energy of alkylammonium-modified montmorillonite and the relation to exfoliation in nanocomposites: Influence of cation density, head group structure, and chain length. *Chemistry of Materials*, **22**, 1595–1605.
- Fu Y.T. & Heinz H. (2010b) Structure and cleavage energy of surfactant-modified clay minerals: Influence of CEC, head group, and chain length. *Philosophical Magazine*, **90**, 2415–2424.
- Fu Y.T., Zartman G.D., Yoonessi M., Drummy L.F. & Heinz H. (2011) Bending of layered silicates on the nanometer scale: mechanism, stored energy, and curvature limits. *The Journal of Physical Chemistry C*, **115**, 22292–22300.
- Gaines G.L., Jr. (1957) The ion-exchange properties of muscovite mica. *The Journal of Physical Chemistry*, **61**, 1408–1413.
- Giese R.F. & van Oss C.J. (2002) *Colloid and Surface Properties of Clays and Related Minerals*. Dekker, New York.
- Giese R.F., Constanzo P.M. & van Oss C.J. (1991) The surface free energies of talc and pyrophyllite. *Physics and Chemistry of Minerals*, **17**, 611–616.
- Greathouse J.A., Refson K. & Sposito G. (2000) Molecular dynamics simulation of water mobility in magnesium-smectite hydrates. *Journal of the American Chemical Society*, **122**, 11459–11464.
- Greenwell H.C., Harvey M.J., Boulet P., Bowden A.A., Coveney P.V. & Whiting A. (2005) Interlayer structure and bonding in nonswelling primary amine intercalated clays. *Macromolecules*, **38**, 6189–6200.
- Habelitz S., Carl G., Rüssel C., Theil S., Gerth U., Schnapp J. D., Jordanov A. & Knake H. (1997) Mechanical properties of oriented mica glass ceramic. *Journal of Non-Crystalline Solids*, **220**, 291–298.
- Hackett E., Manias E. & Giannelis E.P. (1998) Molecular dynamics simulations of organically modified layered silicates. *Journal of Chemical Physics*, **108**, 7410–7415.
- Hayes W.A. & Schwartz D.K. (1998) Two-stage growth of octadecyltrimethyl-ammonium bromide monolayers at mica from aqueous solution below the Krafft point. *Langmuir*, **14**, 5913–5917.
- He H.P., Galy J. & Gerard J.F. (2005) Molecular simulation of the interlayer structure and the mobility of alkyl chains in HDTMA<sup>+</sup>/montmorillonite hybrids. *Journal of Physical Chemistry B*, **109**, 13301–13306.
- Heinz H. (2010) Computational screening of biomolecular adsorption and self-assembly on nanoscale surfaces. *Journal of Computational Chemistry*, **31**, 1564–1568.
- Heinz H. & Suter U.W. (2004a) Surface structure of organoclays. *Angewandte Chemie*, **43**, 2239–2243.
- Heinz H. & Suter U.W. (2004b) Atomic charges for classical simulations of polar systems. *The Journal of Physical Chemistry B*, **108**, 18341–18352.
- Heinz H., Castelijns H.J. & Suter U.W. (2003) Structure and phase transitions of alkyl chains on mica. *Journal of the American Chemical Society*, **125**, 9500–9510.
- Heinz H., Paul W., Binder K. & Suter U. W. (2004) Analysis of the phase transitions in alkyl-mica by density and pressure profiles. *Journal of Chemical Physics*, **120**, 3847–3854.
- Heinz H., Koerner H., Anderson K.L., Vaia R.A. & Farmer B.L. (2005) Force field for mica-type silicates and dynamics of octadecylammonium chains grafted to montmorillonite. *Chemistry of Materials*, **17**, 5658–5669.
- Heinz H., Vaia R.A. & Farmer B.L. (2006) Interaction energy and surface reconstruction between sheets of layered silicates. *Journal of Chemical Physics*, **124**, 224713.
- Heinz H., Vaia R.A., Krishnamoorti R. & Farmer B.L. (2007) Self-assembly of alkylammonium chains on montmorillonite: Effect of chain length, headgroup structure, and cation exchange capacity. *Chemistry of Materials*, **19**, 59–68.
- Heinz H., Vaia R.A. & Farmer B.L. (2008a) Relation between packing density and thermal transitions of alkyl chains on layered silicate and metal surfaces.

- Langmuir*, **24**, 3727–3733.
- Heinz H., Vaia R.A., Koerner H. & Farmer B.L. (2008b) Photoisomerization of azobenzene grafted to montmorillonite: Simulation and experimental challenges. *Chemistry of Materials*, **20**, 6444–6456.
- Herrero C.P. & Sanz J. (1991) Short-range order of the Si,Al distribution in layer silicates. *Journal of Physics and Chemistry of Solids*, **52**, 1129–1135.
- Hill R.J. (1979) Crystal structure refinement and electron density distribution in diaspora. *Physics and Chemistry of Minerals*, **5**, 179–200.
- Iyi N., Fujita T., Yelamagad C.V. & Lopez Arbeloa F. (2001) Intercalation of cationic azobenzene derivatives in a synthetic mica and their photoresponse. *Applied Clay Science*, **19**, 47–58.
- Jacobs J.D., Koerner H., Heinz H., Farmer B.L., Mirau P., Garrett P.H. & Vaia R.A. (2006) Dynamics of alkyl ammonium intercalants within organically modified montmorillonite: dielectric relaxation and ionic conductivity. *The Journal of Physical Chemistry B*, **110**, 20143–20157.
- Kamal M.R., Calderon J.U. & Lennox R.B. (2009) Surface energy of modified nanoclays and its effect on polymer/clay nanocomposites. *Journal of Adhesion Science Technology*, **23**, 663–688.
- Kunz D.A., Max E., Weinkamer R., Lunkenbein T., Breu J. & Fery A. (2009) Deformation measurements on thin clay tactoids. *Small*, **5**, 1816–1820.
- Kuppa V. & Manias E. (2002) Computer simulation of PEO/layered silicate nanocomposites: 2. Lithium dynamics in PEO/Li<sup>+</sup> montmorillonite intercalates. *Chemistry of Materials*, **14**, 2171–2175.
- Lagaly G. (1976) Kink-block and gauche-block structures of bimolecular films. *Angewandte Chemie International Edition*, **15**, 575–586.
- Lagaly G. & Dekany I. (2005) Adsorption on hydrophobized surfaces: clusters and self-organization. *Advances in Colloid and Interface Science*, **114**, 189–204.
- Lagaly G. & Weiss A. (1970) Arrangement and orientation of cationic tensides on silicate surfaces. 2. Paraffin-like structures in alkylammonium layer silicates with a high layer charge (mica). *Kolloid-Zeitschrift und Zeitschrift für Polymere*, **237**, 364–368.
- Lagaly G. & Weiss A. (1971) Arrangement and orientation of cationic tensides on silicate surfaces. 4. Arrangement of alkylammonium ions in low-charged silicates in films. *Kolloid-Zeitschrift und Zeitschrift für Polymere*, **243**, 48–55.
- Lee J.H. & Guggenheim S. (1981) Single crystal X-ray refinement of pyrophyllite-1Tc. *American Mineralogist*, **66**, 350–357.
- Lewin M., Mey-Marom A. & Frank R. (2005) Surface free energies of polymeric materials, additives, and minerals. *Polymers for Advanced Technologies*, **16**, 429–441.
- Lewis J., Schwarzenbach D. & Flack H.D. (1982) Electric field gradients and charge density in corundum,  $\alpha$ -Al<sub>2</sub>O<sub>3</sub>. *Acta Crystallographica Section A*, **A38**, 733–739.
- Lin F.H., Lee Y.H., Jian C.H., Wong J.M., Shieh M.J. & Wang C.Y. (2002) A study of purified montmorillonite intercalated with 5-fluorouracil as drug carrier. *Biomaterials*, **23**, 1981–1987.
- Lipsicas M., Raythatha R.H., Pinnavaia T.J., Johnson I.D., Giese R.F., Constanzo P.M. & Robert J.L. (1984) Silicon and aluminium site distribution in 2:1 layered silicate clays. *Nature*, **309**, 604–607.
- Mazo M.A., Manevitch L.I., Gusarova E.B., Shamaev M.Y., Berlin A.A., Balabaev N.K. & Rutledge G.C. (2008) Molecular dynamics simulation of thermo-mechanical properties of montmorillonite crystal. 1. Isolated clay nanoplate. *The Journal of Physical Chemistry B*, **112**, 2964–2969.
- McNeil L.E. & Grimsditch M. (1993) Elastic moduli of muscovite mica. *Journal of Physics: Condensed Matter*, **5**, 1681–1690.
- Michot L.J., Villieras F., Francois M., Yvon J., LeDred R. & Cases J.M. (1994) The structural microscopic hydrophilicity of talc. *Langmuir*, **10**, 3765–3773.
- Mooney R.W., Keenan A.G. & Wood L.A. (1952a) Adsorption of water vapor by montmorillonite. I. Heat of desorption and application of BET theory. *Journal of the American Chemical Society*, **74**, 1367–1374.
- Mooney R.W., Keenan A.G. & Wood L.A. (1952b) Adsorption of water vapor by montmorillonite. II. Effect of exchangeable ions and lattice swelling as measured by X-ray diffraction. *Journal of the American Chemical Society*, **74**, 1371–1374.
- Ngo T. & Schwarzenbach D. (1979) The use of electric field gradient calculations in charge density refinements. II. Charge density refinement of the low-quartz structure of aluminum phosphate. *Acta Crystallographica Section A*, **A35**, 658–664.
- Ogawa M., Ishii T., Miyamoto N. & Kuroda K. (2001) Photocontrol of the basal spacing of azobenzene-magadiite intercalation compound. *Advanced Materials*, **13**, 1107–1109.
- Ogawa M., Ishii T., Miyamoto N. & Kuroda K. (2003) Intercalation of a cationic azobenzene into montmorillonite. *Applied Clay Science*, **22**, 179–185.
- Okada T., Watanabe Y. & Ogawa, M. (2005) Photoregulation of adsorption behavior of phenol for azobenzene-clay intercalation compounds. *Journal of Materials Chemistry*, **15**, 987–992.
- Osman M.A. & Suter U.W. (1999) Dodecyl pyridinium alkali metals ion exchange on muscovite mica. *Journal of Colloid and Interface Science*, **214**, 400–406.
- Osman M.A. & Suter U.W. (2000) Determination of the cation-exchange capacity of muscovite mica.

- Journal of Colloid and Interface Science*, **224**, 112–115.
- Osman M.A., Moor C., Caseri W.R. & Suter U.W. (1999) Alkali metals ion exchange on muscovite mica. *Journal of Colloid and Interface Science*, **209**, 232–239.
- Osman M.A., Seyfang G. & Suter U.W. (2000) Two-dimensional melting of alkane monolayers ionically bonded to mica. *The Journal of Physical Chemistry B*, **104**, 4433–4439.
- Osman M.A., Ernst M., Meier B.H. & Suter U.W. (2002) Structure and molecular dynamics of alkane monolayers self-assembled on mica platelets. *The Journal of Physical Chemistry B*, **106**, 653–662.
- Osman M.A., Ploetze M. & Skrabal P.J. (2004) Structure and properties of alkylammonium monolayers self-assembled on montmorillonite platelets. *The Journal of Physical Chemistry B*, **108**, 2580–2588.
- Osman M.A., Rupp J.E.P. & Suter U.W. (2005) Gas permeation properties of polyethylene-layered silicate nanocomposites. *Journal of Materials Chemistry*, **15**, 1298–1304.
- Pandey R.B., Anderson K.L., Heinz H. & Farmer B.L. (2005) Conformation and dynamics of a self-avoiding sheet: bond-fluctuation computer simulation. *Journal of Polymer Science B*, **43**, 1041–1046.
- Pandey R.B., Heinz H., Farmer B.L., Drummy L.F., Jones S.E., Vaia R.A. & Naik R.R. (2010) Layer of clay platelets in a peptide matrix: Binding, encapsulation and morphology. *Journal of Polymer Science B*, **48**, 2566–2574.
- Parbhakar A., Cuadros J., Sephton M. A., Dubbin W., Coles B. J. & Weiss D. (2007) Adsorption of L-lysine on montmorillonite. *Colloids and Surfaces A: Physicochemical and Engineering Aspects*, **307**, 142–149.
- Patwardhan S.V., Emami F.S., Berry R.J., Jones S.E., Naik R.R., Deschaume O., Heinz H. & Perry C.C. (2012) Chemistry of aqueous silica nanoparticle surfaces and the mechanism of selective peptide adsorption. *Journal of the American Chemical Society*, **134** (published online).
- Paul D.R. & Robeson L.M. (2008) Polymer nanotechnology: Nanocomposites. *Polymer*, **49**, 3187–3204.
- Pawley A.R., Clark S.M. & Chinnery N.J. (2002) Equation of state measurements of chlorite, pyrophyllite, and talc. *American Mineralogist*, **87**, 1172–1182.
- Pospisil M., Capkova P., Merinska D., Malac Z. & Simonik J. (2001) Structure analysis of montmorillonite intercalated with cetylpyridinium and cetyltrimethylammonium: Molecular simulations and XRD analysis. *Journal of Colloid and Interface Science*, **236**, 127–131.
- Pospisil M., Kalendova A., Capkova P., Simonik J. & Valaskova M. (2004) Structure analysis of intercalated layer silicates: Combination of molecular simulations and experiment. *Journal of Colloid and Interface Science*, **277**, 154–161.
- Ray S.S. & Bousmina M. (2005) Biodegradable polymers and their layered silicate nanocomposites: In greening the 21st century materials world. *Progress in Materials Science*, **50**, 962–1079.
- Rothbauer R. (1971) Untersuchung eines 2M<sub>1</sub>-Muskovits mit Neutronenstrahlen. *Neues Jahrbuch für Mineralogie., Monatshefte*, 143–154.
- Sachse W. & Ruoff A.L. (1975) Elastic moduli of precompressed pyrophyllite used in ultrahigh-pressure research. *Journal of Applied Physics*, **46**, 3725–3730.
- Sanz J. & Serratos J.M. (1984) <sup>29</sup>Si and <sup>27</sup>Al high-resolution MAS-NMR spectra of phyllosilicates. *Journal of the American Chemical Society*, **106**, 4790–4793.
- Sato H., Yamagishi A. & Kawamura K. (2001) Molecular simulation for flexibility of a single clay layer. *The Journal of Physical Chemistry B*, **105**, 7990–7997.
- Schoonheydt R.A. & Johnston C.T. (2007) Surface and interface chemistry of clay minerals. Pp. 87–112 in: *Handbook of Clay Science I*. (F. Bergaya & B.K.G. Theng, editors). Elsevier Science Ltd, Amsterdam.
- Schoonheydt R.A. & Johnston C.T. (2011) The surface properties of clay minerals. Pp. 335–370 in: *Layered Mineral Structures and their Application in Advanced Technologies* (M.F. Brigatti & A. Mottana, editors). The European Mineralogical Union.
- Simmons G. & Wang H. (1971) *Single Crystal Elastic Constants and Calculated Aggregate Properties: A Handbook*, 2nd edition. MIT Press, Cambridge, MA.
- Smyth J.R., Jacobsen S.D., Swope R.J., Angel R.J., Arlt T., Domanik K. & Holloway J.R. (2000) *European Journal of Mineralogy*, **12**, 955–963.
- Suter J.L. & Coveney P.V. (2009) Materials properties of clay nanocomposites: onset of negative Poisson ratio in large-scale molecular dynamics simulation. *Soft Matter*, **5**, 3896–3904.
- Teppen B.J., Rasmussen K., Bertsch P.M., Miller D.M. & Schafer L. (1997) Molecular dynamics modeling of clay minerals. 1. Gibbsite, kaolinite, pyrophyllite, and beidellite. *The Journal of Physical Chemistry B*, **101**, 1579–1587.
- Usuki A., Kojima Y., Kawasumi M., Okada A., Fukushima Y., Kurauchi T. & Kamigaito O. (1993) Synthesis of Nylon-6-Clay Hybrid. *Journal of Materials Research*, **8**, 1179–1184. [A similar contribution was first reported at the Fall National Meeting of the American Chemical Society, 1987].
- Vaia R.A., Teukolsky R.K. & Giannelis E.P. (1994) Interlayer structure and molecular environment of alkylammonium layered silicates. *Chemistry of Materials*, **6**, 1017–1022.

- Vaia R.A. & Giannelis E.P. (1997) Polymer melt intercalation in organically-modified layered silicates: Model predictions and experiment. *Macromolecules*, **30**, 8000–8009.
- Van Olphen H. (1977) *An Introduction to Clay Colloidal Chemistry*. Wiley, New York.
- Vanorio T., Prasad M. & Nur A. (2003) Elastic properties of dry clay mineral aggregates, suspensions, and sandstones. *Geophysical Journal International*, **155**, 319–326.
- Vaughan M.T. & Guggenheim S. (1986) Elasticity of muscovite and its relationship to crystal structure. *Journal of Geophysical Research*, **91**, 4657–4664.
- Weiss A., Mehler A. & Hofmann U. (1956) Organophile vermiculite. *Zeitschrift für Naturforschung*, **11b**, 431–434.
- Yariv S. & Cross H., editors (2002) *Organo-Clay Complexes and Interactions*. Dekker, New York.
- Zartman G.D., Liu H., Akdim B., Pachter R. & Heinz H. (2010) Nanoscale tensile, shear, and failure properties of layered silicates as a function of cation density and stress. *The Journal of Physical Chemistry C*, **114**, 1763–1772.
- Zeng Q.H., Yu A.B., Lu G.Q. & Standish R.K. (2004) Molecular dynamics simulation of the structural and dynamic properties of dioctadecyldimethyl ammoniums in organoclays. *The Journal of Physical Chemistry B*, **108**, 10025–10033.
- Zhu J.X., He H.P., Zhu L.Z., Wen X.Y. & Deng F.J. (2005) Characterization of organic phases in the interlayer of montmorillonite using FTIR and <sup>13</sup>C NMR. *Journal of Colloid and Interface Science*, **286**, 239–244.